A Framework for the Identification of Human Vertical Displacement Activity Based on Multi-Sensor Data

Ajaykumar Manivannan, Elias J. Willemse, Balamurali B. T., Wei Chien Benny Chin, Yuren Zhou, Bige Tunçer, Alain Barrat, and Roland Bouffanais, *Member, IEEE*

***Abstract*—To date, the methodology to track and identify vertical movement from large-scale unstructured data sets is lacking. Here, we design and develop such a framework to accurately and systematically identify the sparse human vertical displacement activity typically buried into the predominantly horizontal mobility. Our framework uses sensor data from a barometer, accelerometer, and Wi-Fi scanner coupled with an extraction step involving a combination of feature engineering and data segmentation. This methodology is subsequently integrated into a machine-learning-based classifier to automatically distinguish vertical displacement activity—with 98% overall accuracy and a 92% F1-score—from its horizontal counterpart. We illustrate the potential of this framework by applying it to an unstructured large-scale data set associated with over 16,000 participants going about their daily activity in the city-state of Singapore. With the vertical movements of this large group uncovered, we can analyze the specific features of this activity class using its statistical distribution. This new knowledge would have significant ramifications for the architectural design of vertical cities.**

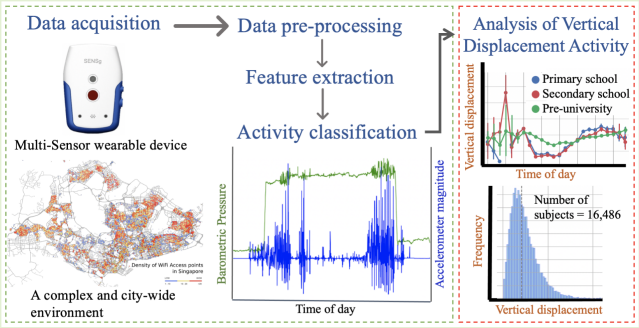

***Index Terms*— Wearable sensors, barometer, multi-sensor identification, human activity recognition, vertical displacement activity, stair climbing.**

Manuscript received January 27, 2022; revised February 24, 2022; accepted March 6, 2022. Date of publication March 8, 2022; date of current version April 14, 2022. This work was supported in part by the Singapore National Research Foundation (NRF), in part by the Ministry of Education (MOE), and in part by the Singapore University of Technology and Design (SUTD)-Massachusetts Institute of Technology (MIT) International Design Centre through National Science Experiment (NSE) 2016. The work of Ajaykumar Manivannan was supported by the Ministry of Education (MOE)-Singapore University of Technology and Design (SUTD) Ph.D. Fellowship and currently supported by the University of Ottawa Ph.D. Admission Scholarship. The associate editor coordinating the review of this article and approving it for publication was Prof. Shih-Chia Huang. *(Corresponding author: Roland Bouffanais.)*

Ajaykumar Manivannan and Roland Bouffanais are with the Department of Mechanical Engineering, University of Ottawa, Ottawa, ON K1N 6N5, Canada (e-mail: roland.bouffanais@uottawa.ca).

Elias J. Willemse is with Waste Labs Pte. Ltd., Singapore 059915.

Balamurali B. T. is with the Engineering Systems and Design (ESD), Singapore University of Technology and Design (SUTD), Singapore 487372.

Wei Chien Benny Chin and Yuren Zhou are with the Engineering Product Development (EPD), Singapore University of Technology and Design (SUTD), Singapore 487372.

Bige Tunçer is with the Architecture and Sustainable Design (ASD), Singapore University of Technology and Design (SUTD), Singapore 487372.

Alain Barrat is with CNRS, CPT, Aix Marseille Univ, Université de Toulon, 13009 Marseille, France, and also with the Tokyo Tech World Research Hub Initiative (WRHI), Tokyo Institute of Technology, Yokohama 226-8503, Japan.

Digital Object Identifier 10.1109/JSEN.2022.3157806

I. Introduction

THE urbanization of our planet is rapidly increasing, with 55% of the world population now living in cities [1]. In 2030, this number is projected to increase to 60% [1]. In the face of this unabated urbanization trend, cities struggle to accommodate the population influx through urban sprawl alone, primarily because of land scarcity and the induced strain on transportation networks. An alternative to urban sprawl currently predominant in the rapidly urbanizing Asia is increasing the density of the built environment, inevitably leading to cities with vertically dominated landscapes and singular skylines.

Such vertical cities exhibit a very distinct urban landscape, manifesting a sprawl of an upward nature with a very high density of high-rise buildings—not necessarily limited to skyscrapers. This vertical growth of cities is reflected in the increasing market demand around the world for vertical transportation systems like elevators and escalators, with approximately 100,000 units installed in 2019 and a forecast for 250,000 units commissioned in 2024 alone [2]. The Asia-Pacific region, where most of the fastest-growing cities in the world are present [1], is said to have the highest growth in demand (85%) for vertical transportation systems [2].

Over the last half-century, today's urban planning has dramatically benefited from extensive human mobility studies. Over the last two decades, this area of research has experienced significant growth due to the convergence of several technological factors: (1) the development of new sensors enabling more accurate tracking of human mobility, (2) the very rapid and massive adoption of mobile phones globally, and (3) the so-called "Big Data" effect. In addition, complexity scientists have developed several new frameworks to analyze and identify specific mobility patterns. Those patterns hidden in troves of high-resolution mobility data have been uncovered thanks to large-scale experiments or from massive commercial databases—e.g., call detailed record (CDR) [3]. However, it is essential to note that these human mobility studies are limited to horizontal movements, i.e., based on a two-dimensional representation of the urban landscape. Roads, railway networks, and pedestrian pathways are modeled on a planar surface in these studies.

As already mentioned, the rapid change in the topology of cities in the developing world, especially in Asia, is prominently three-dimensional [4]. Therefore, the development of sustainable and livable cities heavily depends on studies of human mobility across all three dimensions. However, while brand-new skyscrapers are being erected every day globally, we know surprisingly little about vertical human mobility. For instance, some recent studies propose to study vertical displacements in vertically integrated mixed-use developments as a means to identify key spatial connectors that have a direct influence on social interactions [5]. Moreover, a systematic study of vertical human mobility would benefit urban/infrastructure planning in many ways: e.g., targeted facility allocation in high-rise buildings, optimal placement of vertical nodes based on the typology of the building and the estimated vertical transportation load, effective vertical integration of a building in its neighborhood, etc. [6].

Horizontal mobility has been extensively studied using a wide variety of data sources: e.g., census data, travel surveys, CDR, location-based social network services, GPS [7], and smart travel/transit cards [8]. However, none of these approaches and sensors can effectively track vertical displacements. Interestingly, the sensor technology required to track such human vertical mobility accurately is readily available. What is missing is a methodology that enables the accurate identification of various types of possible vertical displacements from the output of large-scale human experiments with sufficient statistical significance.

Here, we report a contribution towards that goal by introducing and validating a methodology to accurately and systematically identify the sparse human vertical displacement activity (VDA) [9] that is deeply embedded within the predominantly horizontal displacement activity. This methodology is then integrated into a machine-learning-based classifier capable of dealing with large-scale data sets collected in free-living and unstructured urban environments. Classically, barometers have been the primary type of sensor used to track motion in the vertical direction. Indeed, barometric pressure—possibly augmented by other sensors—is commonly used in the field of Human Activity Recognition (HAR) to recognize the particular VDA class, which is of prime interest to us [9]. Specifically, VDA is a particular human activity class that deals with the vertical displacement of individuals in the built environment through commonly available modes of vertical mobility such as stairs, escalators, elevators, or slopes. In this work, the term VDA is intended to encompass human movements in vertically built structure solely. That means we are discarding changes in elevation associated with any vehicle motion (motor vehicle, train, bicycle, cable car, etc.).

Our methodological advancement is thoroughly tested and validated using a big data set obtained from a large-scale human experiment carried out in Singapore: the so-called National Science Experiment (NSE). The NSE was a city-scale experiment that involved 50,000 students in Singapore between 2015 and 2017. The wearable devices designed explicitly for this large-scale experiment were carried by students continuously for five days and contained several sensors, including a barometer and an accelerometer. By fully understanding the complex interplay of factors that influence barometric pressure, we develop several preprocessing methods to alleviate the effects of those factors, with the end goal of achieving the highest possible accuracy in the VDA identification process. Moreover, the VDA extraction process must be robust enough to handle inherent limitations associated with such large-scale human experiments—i.e., low sampling rate, heterogeneity in devices and participant population, missing data, and sensor errors. As part of this process, we manually label a large number of training data (81 subjects, 81 devices, for a time period of 24 hours). This step is followed by a validation using a short-term video-annotated data set (2 subjects, 5 devices, for a period of 6 hours). Finally, we integrated the developed VDA identification methodology into a machine-learning-based classifier. Subsequently, we applied it to the large-scale NSE data set to extract unique features of human vertical mobility associated with the student population participating in the NSE.

The main contributions of this paper can be summarized as follows (see Fig. 1):

- A novel and accurate multi-sensory identification of vertical displacement activity is developed and validated against a sparse data set from a large-scale human experiment involving over 16, 000 individuals going about their daily activity within a densely urban environment.
- The accuracy of this VDA identification process is found to be strongly dependent on a several constraints associated with the sensing of key physical quantities. Specifically, we design a feature extraction step involving a combination of feature engineering and data segmentation. In addition, the properties of the sensors and how they are used in such large-scale experiments create many challenges, which are identified and addressed.
- Using our novel VDA identification process, a machine-learning-based classifier allows us to carry out the first large-scale analysis of human vertical mobility in a city-scale experiment. Interestingly, our results reveal a highly heterogeneous distribution of vertical activity, both in terms of the number of events and of the size of vertical

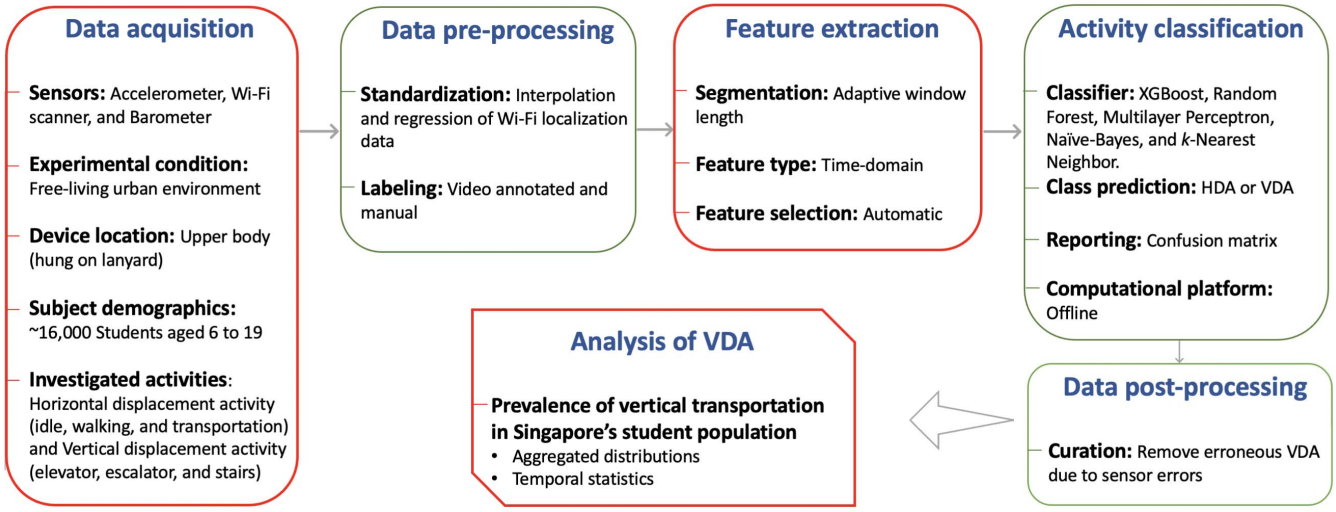

Fig. 1. Human activity recognition (HAR) process in the identification of VDA [10]. This flowchart describes the overall process developed to achieve our VDA analysis represented in the last rectangular box. The key contributions of this work are in the boxes with a red outline.

jumps. These results have far-reaching implications for the architectural design of dense urban environments.

II. Related Works

In the field of HAR, sensor data requires preprocessing followed by the application of recognition models to classify the activity classes of interest [11], [12]. Algorithms for identifying VDA from sensor data range from simple threshold-based models to sophisticated Machine Learning (ML) algorithms like deep learning. In the present work, we employ an ML-based classification model, and we review here several prior studies concerning the use of ML to classify VDA events.

One of the pioneering works on identifying VDA was performed in 1998 by Sagawa *et al.* [13], using accelerometer and barometer data to identify VDA. The study used a threshold-based model with a small training sample (83 minutes and 6 subjects). Since then, the combined effects of the digital revolution, the ubiquity of mobile devices, and the advances in sensors, Big Data, and ML have paved the way for the possibility of real-time recognition of activity classes of individuals evolving in complex environments.

Accelerometers are the most widely used sensors to track human activities [14]–[16]. Studies using an accelerometer as the stand-alone sensor show that the prevalent mode of tracked vertical mobility is stairs climbing [11], [17]–[23]. However, the classification accuracy of stairs climbing tends to be lower than other activity classes [24], [25]. This led researchers to include additional data sources to improve the accuracy of VDA detection, such as gyroscope, magnetometer, and barometer data [26]–[30], consider other modes of vertical mobility such as escalator and elevator rides. For instance, Liu *et al.* [26] added barometer data to a model that used accelerometer, gyroscope, and magnetometer sensor data, notably improving the classification accuracy from $\sim 80\%$ to $\sim 90\%$ (number of subjects: 10).

Additionally, some studies have acknowledged that accelerometers are effectively less robust than barometers for VDA classification. For example, Muralidharan *et al.* [31] compared the VDA recognition performance using an accelerometer versus a barometer and showed that their VDA classification performances were similar — with the barometer-based framework performing slightly better at nearly 100% accuracy (number of subjects: 2). However, the accuracy of the accelerometer-based framework dropped drastically when the mobile device was used to take calls or play games [31]. Similarly, Vanini *et al.* [32] showed that the classification performance of VDA was comparable for accelerometer-only and barometer-only study ($\sim$ 99%), but that the barometer was more energy-efficient and less dependent from the on-body position than accelerometers (number of subjects: 10).

Our study focuses on recognizing VDA as a general class of activity. It uses the following sensor data: (1) location data derived from Wi-Fi Access Points (APs), (2) magnitude of 3-axis accelerometer, and (3) barometric pressure data.

The magnitude of the 3-axis accelerometer signal is orientation independent [33], [34] and does not require complex data post-processing [11]. On the other hand, raw barometric sensor data can entail noise introduced by random sensor errors, limited sensor resolution, and high sampling frequency ($>$ 2 Hz). Filtering techniques like moving average filters [35]–[37], Finite Impulse Response (FIR) filters [38], and Infinite Impulse Response (IIR) filters [27], [38]–[40] are commonly used to alleviate the noise effects. Signal modeling such as sinusoidal fitting [41] and sigmoidal nonlinear fitting [42] is used to increase the precision in extracting elevation changes. In the present study, the spectral resolution of the sensor data collection is 0.06 Hz. Such a low sampling rate allows the system to side-step noise appearing at a high sampling rate that affects precise extraction of elevation changes. Therefore, the barometric pressure sensor data we consider here are not filtered, and other noise sources due to sensor resolution are used to quantify the uncertainty in the magnitude of the predicted VDA.

Barometric pressure data is usually converted to several common feature types such as: (1) statistical [43], [44], (2) spectral [43]–[45], (3) temporal [43], [44], and (4) wavelet-based features [46], [47]. The most commonly used fea-

tures are the rate of change of pressure (vertical velocity or slope) [26], [35], [43], [48], [49] and differential pressure (dp) [48], [50].

Vanini *et al.* [32] used barometric pressure data alone to recognize VDA using the features–rate of change of pressure and the standard deviation of differential pressure. They found that Long Short-Term Memory (LSTM) neural network framework produces a 99% accuracy compared to a decision tree approach (96%) and naïve Bayes classifiers (93%). However, their data collection was of short duration (30 minutes for each class) and conducted in limited environments. Muralidharan *et al.* [31] detected floor changes with an accuracy of 99% using the J48 decision tree model. Even though several factors that affect barometric pressure are considered, the data collected were of short duration (few minutes), conducted in limited structured environments, and lacked any entanglement with transportation modes. Liu *et al.* [26] classified vertical displacement activities from horizontal displacement activities (HDA) using inertial measurement units (IMU, including magnetometer) and barometer sensor data, with barometric sensor features derived from the standard deviation of pressure and rate of change of pressure. By training various classifiers such as Random Forest, J48 decision trees, Artificial Neural Networks (ANN), SVM, and Naïve Bayes, they obtained that Random Forest classifiers produced the highest accuracy of 92%. Also, in this study, each activity class was performed only for a few minutes and limited to ambulation [26].

The review of the literature on HAR [11], [12], [51]–[54] makes it clear that no classifier can be considered the best one universally, i.e. without considering the context in which it is used. As each data set comes with its own set of distinct characteristics, the classifier working best for a particular data set and activity type might not have the best performance for a specific problem or different circumstances (i.e., not generalizable) [11]. In this study, we have chosen two ensemble models (XGBoost and Random Forest), a neural network model (Multilayer perceptron) a Bayesian model (Naive-Bayes), and an instance-based nearest-neighbor model (k-Nearest Neighbor) to evaluate and compare the performances of each model on our data set (see Fig. 1).

It is common in the HAR literature to use short-duration training data collected in segments that contain only one or two activity classes and are performed in semi-natural or laboratory conditions, with limited variability in environments. However, real-life human activities occur in complex and unstructured environments, with a wide range of possible sequences, spanning heterogeneous activity classes with heterogeneous durations. Our study collocates itself in such a framework, as it uses a long-term (5 days) data set collected in a large-scale student population ($\sim 50,000$ students) during their regular weekdays. Hence, it requires a different approach than those reported in the literature.

Indeed, long-term monitoring of human activities requires a thorough understanding of all the factors affecting the sensor data in different static and dynamic environments. In particular, the factors that influence barometric pressure data are climate and weather, air velocity during motion, built environment, altitude, and sensor accuracy [9]. For a detailed review on the use of barometers to track human activity and the many factors that affect barometric pressure, we refer the reader to the recent review paper [9].

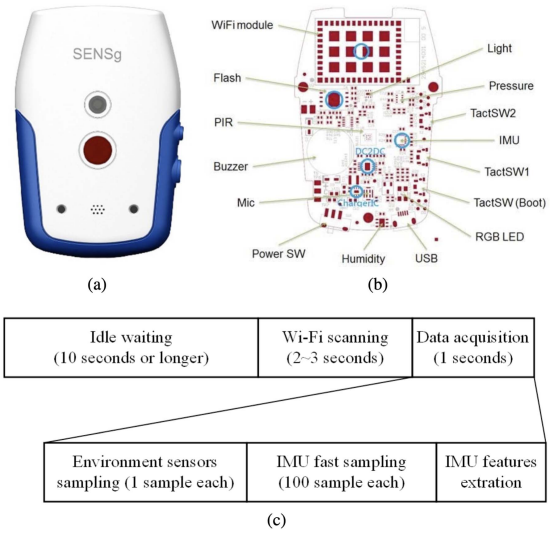

Fig. 2. NSE SENSg device details: (a) outside look, (b) internal structure [56], (c) working cycle. (Picture Courtesy: [57]).

III. Description of Data

A. National Science Experiment Data

The National Science Experiment (NSE) was designed and commissioned by the Singapore National Research Foundation (NRF) and the Singapore University of Technology and Design (SUTD), with other private and government bodies in Singapore [55]. The primary objective of this island-wide science experiment carried out by Singapore students—themed "Step Out for Science"—was to monitor and evaluate their carbon footprint, travel mobility patterns, amount of time spent indoors and outdoors, and more.

Almost $50,000$ students from 92 schools distributed nation-wide participated in the NSE in 2016 (Table I). Each student carried a wearable device called SENSg (see Fig. 2), which consisted of built-in environmental, motion sensors, and communication units. The devices were able to record and transmit the sensed data related to the Activities of Daily Living (ADL) of the students to a cloud server [56]. The data was recorded every $13 \sim 18$ seconds over weekdays, from Monday to Friday, for eight weeks in 2016. The device goes to sleep mode to reduce battery consumption when the processed IMU signal shows no user movement. The SENSg devices were handed over to the students on Mondays and collected back on Fridays. Hence, the full-time scale of daily ADL is only available on Tuesdays, Wednesdays, and Thursdays. Table II shows the cleaned NSE 2016 database after removing devices based on two criteria (a) data coverage for less than 6 hours per day (b) percentage of missing location data larger than 50% in a day.

Our study uses the accelerometer, barometer, and Wi-Fi scanners embedded in the SENSg devices to detect students' Vertical Displacement Activities (VDA) during their ADL. These sensor types are widely available in modern

TABLE I
NSE 2016 - DEVICE DELIVERY INFORMATION

Dates	No. schools	No. devices	Primary (6–12 y.o.)	Secondary (12–16 y.o.)	Pre-University (16–19 y.o.)
Apr 11–15	7	3,002	1,590	1,192	220
Apr 18–22	7	3,290	2,300	990	–
May 16–20	10	2,673	820	1,624	229
May 23–27	2	840	–	220	620
July 11–15	32	10,751	3,834	6,677	240
July 18–22	23	7,934	5,233	2,181	520
July 25–29	8	15,029	220	890	13,919
Aug 17–19	3	6,000	–	–	6,000
Total	92	49,519	13,997	13,774	21,748

TABLE II
CURATED NSE 2016 DATABASE

Dates	No. schools	No. IDs	Primary (6–12 y.o.)	Secondary (12–16 y.o.)	Pre-University (16–19 y.o.)
Apr 11–15	7	1,797	1,049	608	140
Apr 18–22	7	1,793	1,265	528	–
May 16–20	10	700	239	386	75
May 23–27	–	–	–	–	–
July 11–15	33	4,387	2,048	2,114	73
July 18–22	21	3,086	2,292	666	128
July 25–29	8	3,345	–	93	3,057
Aug 17–19	3	1,380	–	–	1,380
Total	89	16,581	6,939	4,395	4,853

smartphones, rendering them ideal for this particular HAR. The SENSg device comprises the IMU sensor MPU9250 from InvenSense and the barometer sensor BMP280 from Bosch Sensortech. The device also collected and stored up to a maximum of 20 Wi-Fi Access Points (AP) with the highest Receiver Signal Strength Indication (RSSI). We used Skyhook, a mobile location service from Boston, Massachusetts, that has geolocation of billions of Wi-Fi APs around the world, to convert the Wi-Fi APs to location coordinates [58]. The location coordinates (latitude and longitude) have a typical location accuracy of ± 100 meters. The location accuracy is increased by applying regression to the time-series of location data (see Appendix B). When the Wi-Fi APs are sparse or absent, location data is considered missing. Interpolation is then applied to the time-series data to predict these missing values (see Appendix A). The full sensor characteristics are shown in Table III [56]. The embedded barometer sensor is capable of detecting up to 1-meter changes in height, i.e., ± 12 Pa [56]. The raw values measured by the accelerometer along its three axes were processed on-board the SENSg, and only descriptive statistics of these raw data were recorded: (1) $\max(M_{\text{acc}})$—the maximum value of the accelerometer's signal magnitude (2) $\text{std}(M_{\text{acc}})$—the standard deviation of accelerometer's magnitude, both sampled at 100 Hz during the one-second data acquisition temporal window, which occurred in its turn with frequency ~ 0.0625 Hz. The SENSg device, along with its working cycle, is shown in Fig. 2.

B. Video-Annotated Data

As the measure of the barometric pressure behavior is influenced by many factors, it is vital to have at our disposal

TABLE III
SENSOR CHARACTERISTICS OF SENSG DEVICE

Sensor	Model	Range	Accuracy	Units	Poll frequency
Wi-Fi	SN8205	–	–	–	0.062 Hz
Barometer	BMP280	300 to 1,100 hPa	± 12 Pa	Pa	0.062 Hz
Accelerometer	MPU9250	± 2 g	± 80 mg	mg/LSB	100 Hz (for every 0.062 Hz)

TABLE IV
VIDEO-ANNOTATED DATA

Mode	Total time (hours)
Car	0.4
Bus	1.5
Train	0.7
Cycle	0.8
Walking	1.5
Idle	0.3
VDA	0.4
Total	5.6

a data set with the corresponding ground truth for validation purposes. Therefore, we collected approximately 6 hours of sensor data annotated using video recording to this aim. This data set was recorded across different modes of horizontal (walking, idle, train, bus, car, and cycle) and vertical (elevator, escalator, and stairs) activity (Table IV). Two researchers collected data on different days and times using a SENSg device that was hung using a lanyard similar to the one used by students in the NSE. The video was recorded using a Go Pro Hero 6 mounted on the chest. We will use this data set to validate manual labeling methods described in Sec. IV-A.

IV. METHODOLOGY

As the NSE was conceived as a large-scale data collection with relatively high temporal resolution and for long durations, sensor data collection was optimized to save battery life and data bandwidth. Unfortunately, this compromised sensor resolution, sampling rate, and type of sensor data collected, which inevitably makes the VDA identification more challenging. This section thus details the machine learning framework that we developed to identify and extract VDAs from continuous temporal segments of the NSE data (Fig. 1). Section IV-A explains the manual labeling techniques, and sections IV-B, IV-C, IV-D, and IV-E encompass the machine learning framework. We refer to the Appendices for details related to the pre-processing of the location data (App. A and B), while App. C describes the classification model parameters, and App. D deals with model tuning.

A. Manual Labeling

Accurate annotation of sensor data is highly manpower intensive [59]. One solution is to manually label a small subset of the data based on expertise and validate the classification framework. We were indeed able to perform such a manual

labeling in a subset of the NSE database (see Sec. IV-D), using our general understanding of the factors affecting barometric pressure [9] and leveraging the data annotated with the help of the ground truth video (Sec III-B). In this manual labeling, we labeled each data point as either VDA or HDA, based on the unique characteristic profile of vertical transportation. As noted in [9], pressure changes caused by factors other than vertical transportation are mostly long-term variations (e.g., diurnal pressure cycle) or brief and intense transient spikes (e.g., Indoor-to-outdoor transition).

First, and based on our pilot experiments illustrated in [9], we distinguish VDA from HDA in our manual labeling by monitoring the following characteristics: (1) a low horizontal travel velocity, (2) body movements picked up by the accelerometer, and (3) an increase or decrease in barometric pressure. We note that high magnitude pressure changes that can be mistaken for VDA occur during transportation modes [9], but these transportation modes can be identified by tracking the location data trend, which should then reveal a high horizontal velocity.

For validation of the procedure, the classifier will be trained on the manually labeled data set and then applied to the data set described in Sec.III-B, for which the ground truth is available.

B. Data Segmentation

We segment the time-series sensor data into regions of significant and minor pressure changes to allow the classifier to focus on the main characteristic of VDA—i.e., the pressure-altitude relation. First, each data point is considered to a have significant pressure change based on a cut-off value ($dp_{i,\text{cut-off}}$), determined by considering three points: (1) we want to discard small pressure jumps that could correspond to other factors that yield pressure changes of similar magnitudes, such as slopes and indoor-outdoor transitions [9], (2) we want to consider pressure changes corresponding to at least 50% of the minimum vertical displacement of a single floor, and (3) the changes need to be consistent with the sensor resolution (± 12 Pa).

The change in pressure (dp_i) for each data point is calculated from the difference of the time-series data $dp_i = P_i - P_{i+1}$, where P_i is the pressure datum at instant t_i. The time interval $dt_i = abs(t_i - t_{i+1})$ associated with dp_i should be less than a cut-off value $dt_{i,\text{cut-off}}$ to consider that data can be missing in times of inactivity, and the resulting variation in pressure values for large values of dt_i might then be due to the diurnal pressure cycle. The consecutive significant pressure changes in the same direction (positive change or negative pressure drop) are then grouped to form a segment, i.e. $S_{P_{i,n+1}} = \{P_i, P_{i+1}, \ldots, P_n, P_{n+1}\}$ for a pressure change sequence of $S_{dp_{i,n+1}} = \{P_i - P_{i+1}, P_{i+1} - P_{i+2}, \ldots, P_n - P_{n+1}\}$. Other features and sensor data are grouped using the same groups of indices as for the segmented pressure sequences.

In the case of manually labeled time-series data set, we first label each data point as either VDA or HDA (Sec. IV-A). Therefore, each segmented data might contain both data points labeled VDA and data points labeled HDA. We thus label each segment using a majority rule, and assigning a VDA label in case of a draw. A perfect data segmentation would allow each VDA segment to indicate a complete VDA event with no false positives or false negatives. The choices of $dt_{i,\text{cut-off}}$ and $dp_{i,\text{cut-off}}$ ultimately determine the performance of this method. Hence, we compute the F_1 score (a.k.a. F-measure of balanced F-score) of capturing a complete VDA event in each segment labeled as VDA in the manually labeled training data for a range of $dt_{i,\text{cut-off}}$ ([30, 50, 90, 120] sec) and $dp_{i,\text{cut-off}}$ ([20, 23, 25, 27, 30] Pa) values (Table V). The best F_1 score is obtained for values $dp_{i,\text{cut-off}}$ and $dt_{i,\text{cut-off}}$ equal to 25 Pa and 120 seconds, respectively. We thus perform the data segmentation with these parameter values, and the final classification described below will be performed on these segmented data.

TABLE V
SELECTION OF DATA SEGMENTATION PARAMETERS BASED ON F_1 SCORE

$dt_{i,\text{cut-off}}$	F_1 score (%)				
120	97.68	98.09	**98.15**	96.98	96.98
90	97.65	98.06	98.12	97.94	96.95
60	97.65	97.99	98.06	97.87	96.88
30	97.14	97.39	97.45	97.23	96.22
$dp_{i,\text{cut-off}}$	20	23	25	27	30

C. Feature Engineering

Model explainability is a growing focus in Machine Learning. Therefore, it is natural to start from features based on domain-specific knowledge to improve explainability. We use our data exploration and our understanding of the sensor data and the target event to be recognized to design several domain-specific features. Specifically, we compute the following features from the accelerometer, barometer, and Wi-Fi localization data.

1) Rate of Pressure Change dp/dt: It accounts for the pace of the VDA. This distinguishes the elevation change based activities from phenomena that unravel over slow temporal scales such as sensor drift and diurnal pressure cycle.

2) Modified Zero-Crossing Rate $\widetilde{zcr}$: The zero-crossing rate zcr is a temporal feature that counts the number of sign changes for a given signal during a particular time window. Here, we modified this feature to count sign changes only if the corresponding magnitude difference in pressure is ≥ 20 Pa. This conditioned $\widetilde{zcr}$ can indeed identify the pressure spikes due to factors such as weather and climate, built environment, air velocity during motion, or sensor accuracy, and distinguish them from one-directional pressure changes that occur during elevation changes.

3) Horizontal Travel Velocity dx/dt: As the location data are recorded latitude and longitude, we use the haversine formula (see Eq (1)) to calculate the great circle distance x between two locations. It is based on the assumption that the Earth is approximately spherical, a valid assumption for small distances such as those measured in the NSE data. The horizontal travel velocity dx/dt plays a crucial role in differentiating significant pressure changes of VDA from transportation-based activities [9]. Specifically, the great-circle distance x between

TABLE VI
PROPERTIES OF THE TRAINING-TEST SPLIT DATA SETS

data set	Ground truth	Size in duration	Number of time-series data points	Number of segmented data	Number of devices	Number of individuals	Number of schools	Pri.	Sec.	Pre-U.
Training (80%)	Manual	64 (days)	207,380	7,132	64	64	64	21	20	23
Test (20%)	Manual	17 (days)	55,092	2,166	17	17	17	8	2	7
Video annotated data	Video recording	6 (hours)	1,262	305	5	2	–	–	–	–

location coordinates (φ_1, λ_1) and (φ_2, λ_2) with φ the latitude, λ the longitude, and r the radius of earth, is given by:

$$x = 2r \arcsin\left(\sqrt{\sin^2\left[\frac{\varphi_2-\varphi_1}{2}\right] + \cos\varphi_1 \cos\varphi_2 \sin^2\left[\frac{\lambda_2-\lambda_1}{2}\right]}\right). \quad (1)$$

4) Statistical Features of Immediate Neighborhood in Time-Series Data N_i: By definition, a VDA event is always preceded and followed by an HDA event. However, during vertical mobility modes like the elevator (and sometimes during escalator rides), a person is potentially standing with no significant body movement. Likewise, during transportation modes such as car, bus, or train travel, the vehicle stops intermittently, leading to low horizontal travel velocity regions. Hence, calculating statistical features over an immediate neighborhood of each data point can entail a sequence of events during and around an activity of interest. More precisely, for each data point i, we compute on the time window $N = \{i-2, i-1, i, i+1, i+2\}$ (of approximate width ~ 80 seconds) and for both the horizontal travel velocity dx/dt and the accelerometer data ($\max(M_{\text{acc}})$ and $\text{std}(M_{\text{acc}})$) the ten following statistics: Minimum, Maximum, Average, Median, Mode, RMS (Root Mean Square), MAD (Median Average Deviation), Standard deviation, Variance, and IQR (Inter Quartile Range).

5) Statistical Features of Segmented Data S_i: Many of the statistical features considered for the immediate neighborhood of time-series data are not suitable for segmented data, as the length of the sequences is typically very small for most VDA events—$2 \sim 4$ or even less ($1 \sim 2$) for transportation modes during which the sign of slope dp/dt changes very often. Hence, we compute only each data segment's mean, median, and mode. This is done both for the original sensor data and for the statistical features of immediate neighborhood in the time series, the modified zero-crossing rate $\widetilde{zcr}$, the horizontal travel velocity dx/dt, and the accelerometer data ($\max(M_{\text{acc}})$, and $\text{std}(M_{\text{acc}})$).

In total, we compute 95 features of the segmented data (Sec IV-B). We refer to this set of features as Feature set-I.

D. Training-Validation-Test Data

The NSE 2016 data set is very diverse in terms of the number of students, unique devices, and the demography of individual participants. Hence, each train-validation-test data set should reflect this diversity. To ensure this, we select the data collected during one day by 81 students from 81 different schools, with an appropriate balance of school types (primary, secondary, and pre-university) and weekdays (limited to Tuesday, Wednesday, and Thursday) to form a representative sample (see Table VI. We manually label this data sample according to the steps described in Section IV. This sample data set is then randomly divided into training (80%) and test set (20%). The data collected by any single device is assigned either to training or testing as a whole (data collected by a single student cannot be split between training or testing). The classifier model is trained on the training set, and a 5-fold cross-validation tunes the model's hyperparameters. Once the best model parameters are identified, it is then tested against the test set for the final performance evaluation.

In addition, to validate the manual labeling, we use the trained classifier model on the video-annotated data described in Sec.III-B.

E. Classification Models

We have selected five commonly used classifiers in HAR [11]: (1) Extreme Gradient Boosting (XGBoost or XGB), (2) Random Forest (RF), (3) Naive-Bayes model (NB), (4) k-Nearest Neighbors (kNN), and (5) Multilayer Perceptron (MLP). Both XGBoost and Random Forest are decision-tree-based ensemble learning algorithms. The XGBoost algorithm is based on the boosting method that adds weak learners sequentially to reduce the model's loss function. In contrast, the Random Forest model is based on the bagging method that adds weak learners in parallel and uses the majority voting model to make final predictions. On the other hand, the Naive-Bayes model is a probabilistic learning algorithm based on Bayes' theorem that assumes strong independence between the features. Furthermore, the k-Nearest neighbor model is non-parametric and uses distance-based measures to find the k-nearest samples and a majority voting model to assign a class. Finally, a Multilayer perceptron is an artificial neural network with a single input and output layer, and at least one hidden layer. Due to its multiple (hidden) layers and its nonlinear activation, MPL is known to be suitable for data that is not linearly separable.

The hyperparameters of these classifiers are tuned through a grid search using a 5-fold cross-validation on feature set-I. A more detailed description of the model parameters and model tuning can be found in App. C and D respectively.

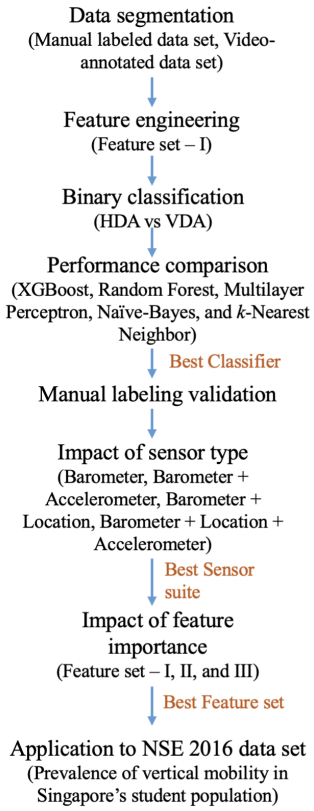

Fig. 3. Flowchart of Sec. V: Results and Discussion.

V. Results and Discussion

The central objective of our study is to obtain the magnitude of vertical displacements of individuals during their daily activities as an indication of vertical movement in a large-scale study of human mobility. By leveraging the relationship between barometric pressure and altitude, our specific aim is to develop pre-processing methods that alleviate the adverse influence of the other factors that affect barometric pressure to extract the instances of vertical motion accurately.

We globally consider the following procedure. First, a small representative sample of the cleaned NSE 2016 data (Sec IV-D) is manually labeled as described in Sec IV-A. We then segment the whole cleaned NSE 2016 data set from Table II and the manually labeled data and video annotated data according to Sec IV-B. The classifier model is then trained on the segmented manually labeled data to achieve a binary classification between Horizontal Displacement Activity (HDA) or Vertical Displacement Activity (VDA). Next, the trained classifier is applied to the video annotated data to validate manual labeling and finally applied to the cleaned NSE 2016 data set (see Fig. 3).

A. Performance Comparison of Classification Models

The four classifiers described in sec. IV-E are trained using feature set-I with the respective hyperparameters tuned from the 5-fold cross-validation with grid search (see Sec. IV-E). Their respective classification performances on the test data set are reported in Table. VIII. The XGBoost model provides the highest overall accuracy (98 %) and F_1-score for classifying VDA (93 %), closely followed by the Random Forest (overall accuracy of 97 % and F_1-score for classifying VDA at 89 %) and the Multilayer perceptron model (overall accuracy of 97 % and F_1-score for classifying VDA at 88 %). The Naive-Bayes model and k-Nearest Neighbor model perform poorly with an F_1-score for classifying VDA standing at 52 % and 17 % respectively. The ensemble learning methods clearly show a superior performance than Naive-Bayes and kNN models, similar to the results reported by Liu *et al.* [26] in classifying VDA from HDA. However, the neural-based MLP also produces similar overall performance as the ensemble learning models while falling slightly short in VDA classification performance. Therefore, we select XGBoost as the classifier of choice for this analysis.

It might be worth adding that future practitioners having access to much larger data sets—possibly with additional sensory features—may consider recent developments in Deep Learning [9], [51], [54], [78] to not only extract VDA but also to discriminate between all VDA types (e.g., escalator riding, staircase climbing, elevator riding).

As shown in Tab. VII, this study considers all the factors that influence barometric pressure with the data set that consisted of both general activity classes—ambulation and transportation—that a user comes across in a natural daily free-living environment and recorded over a long period ($1 \sim 3$ days). As a result, our results show high accuracy in detecting VDA (and HDA) similar to the results reported in the literature while greatly expanding the scope of the identification using the developed framework.

B. Validation of Manual Labeling

The trained XGBoost classifier model is applied to the data set with ground truth annotated from a video recording to ensure the validity of our manual labeling strategies. The results of the classifier performance is shown in Table IX. Although the classifier has 100% precision (i.e., it does not capture false positives), it has a recall of 80% (i.e., it only captures 80% of the actual VDA events), thereby yielding an F1-score of 89%.

The recall performance is relatively low due to a high proportion of instances such that $dp/dt < 1.9$ Pa/sec in the video-annotated data set (16.9% of all points marked as VDA) compared to the test data set (5.5%), for example. This issue is also responsible for some false negatives in the predicted data, where 77% of the predicted false negatives in video-annotated data set have $dp/dt < 1.9$ Pa/sec (see Fig. 4). This is because many of the data points with small pressure jump dp are not labeled as VDA in the manually labeled data set. Indeed, many instances with similar magnitudes for dp cannot be ruled out with high confidence, given the known factors influencing barometric pressure [9].

C. Impact of Sensor Type and Feature Importance

Three sensors are employed for this study: Barometer, tri-axis accelerometer, and Wi-Fi scanner (location data). To understand the impact of these sensor types on the

TABLE VII

CATEGORIZED LITERATURE RELATED TO STUDIES THAT HAVE IDENTIFIED VDA AS PART OF THE ACTIVITY CLASS USING BAROMETER AND ADDITIONAL SENSORS. SENSORS: BAROMETER (BARO), ACCELEROMETER (ACC), MAGNETOMETER (MAG), AND GYROSCOPE (GYRO). FACTORS CONSIDERED: 1. ALTITUDE, 2. CLIMATE AND WEATHER, 3. BUILT ENVIRONMENT, 4. AIR VELOCITY DUE TO MOTION, AND 5. SENSOR ACCURACY. ACTIVITY CLASS: AMBULATION (A) AND TRANSPORTATION (T)

Ref.	Sensors	Factors Considered	Activity Class(es)	Location	Time Period	Best ML model	Overall Accuracy (%)
This work	Baro, Acc, Wifi	1, 2, 3, 4, 5	A & T	Indoor and outdoor	Short and Long	XGBoost	98
[60]	Baro	1, 3, 4	T	Outdoor	Short	Threshold	84
[38]	Baro	1	A	Indoor	Short	Decision Tree	95
[48]	Baro	1, 2, 4, 5	A & T	Indoor and outdoor	Short	Threshold	93
[50]	Baro	1, 2, 3	A	Indoor and outdoor	Short and long	Naive-Bayes	99
[61]	Baro	1, 2, 3, 5	A	Indoor	Short	Threshold	99
[62]	Baro	1, 2, 5	A	Indoor	Long	Hierarchical clustering	98
[35]	Baro	1, 3, 5	A	Indoor	Short	Threshold	95
[31]	Baro	1, 2, 3, 5	A	Indoor	Short and long	J48 Decision Tree	100
[32]	Baro	1, 2, 3, 5	A & T	Indoor and outdoor	Short	Recurrent Neural Network	99
[63]	Baro	1, 2, 3, 4, 5	T	Outdoor	Short and long	DTW	80
[26]	Baro, Acc, Mag, Gyro	1, 2, 3, 5	A	Indoor	Short	Random Forest	92
[64]	Baro, Acc, Gyro	1	A	Indoor	Short	J48 Decision tree	80
[65]	Baro, Acc, Gyro, Mag, WiFi, Microphone	1	A	Indoor and outdoor	Short	Random Forest	85
[66]	Baro, WiFi	1, 2, 5	A	Indoor	Short and long	Monte Carlo Bayesian	97
[67]	Baro, WiFi	1, 2, 5	A	Indoor	Short	Bayesian	96
[27]	Baro, Acc, Gyro	1	A	Indoor	Short	KNN	97
[68]	Baro, Acc	1	A	Indoor	Short	Probabilistic Neural Network and Adjustable Fuzzy Clustering	91
[69]	Baro, Acc	1	A	Indoor	Short	SVM	98
[47]	Baro, Acc, Mag, Gyro	1, 3, 5	A	Indoor and outdoor	Short	SVM and KNN	96
[46]	Baro, Acc	1	A	Indoor	Short	Continuous Wavelet Transform	96
[39]	Baro, Acc	1	A & T	Indoor	Short	Threshold	96
[70]	Baro, Acc	1	A	Indoor and outdoor	Short and long	Decision Tree	97
[42]	Baro, Acc, Gyro, Mag, Foot pressure	1	A	Indoor	Short	Decision Tree	99
[71]	Baro, Acc	1, 5	A + cycling	Indoor and outdoor	Short	Decision Tree	98
[72]	Baro, Acc	1, 2, 3	A	Indoor	Short	Bayesian Network model	99
[73]	Baro, Acc, Gyro	1	A	Indoor	Short	Finite State Machine	NA
[74]	Baro, GPS	1, 2, 3, 4	T	Outdoor	Long	SVM	99
[44]	Baro, Acc	1	A	–	Short	Decision Tree	94
[13]	Baro, Acc	1, 2, 5	A	Indoor	Short	Kalman Filter	95
[75]	Baro, Acc, Mag	1, 3, 5	A	Indoor	Short	KNN and Random Forest	98
[41]	Baro, Acc, Gyro	1, 2	A	Indoor	Short	Decision tree	98
[76]	Baro, WiFi, Bluetooth	1, 2, 5	A	Indoor	Short	Threshold	90
[77]	Baro, Acc, Gyro, Mag, WiFi	1	A	Indoor	Short	Extended Kalman Filter	97
[43]	Acc, Gyro, Mag	1	A	Indoor	Short	Decision tree	90

classification of VDA, we conduct an ablation study. Since barometric pressure data is used in the pre-processing step (data segmentation) and is vital to extracting vertical displacements, features derived from barometer data are not removed

TABLE VIII
COMPARISON OF CLASSIFIER PERFORMANCE ON THE TEST DATA SET WITH FEATURE SET-I

Model	Overall accuracy (%)	Class	Precision (%)	Recall (%)	F_1-score (%)	Support
XGB	98	HDA	99	99	99	1899
		VDA	93	92	93	277
RF	97	HDA	98	99	99	1899
		VDA	96	83	89	277
MLP	97	HDA	98	98	98	1899
		VDA	89	88	88	277
NB	80	HDA	97	80	88	1899
		VDA	38	83	52	277
kNN	87	HDA	88	99	93	1899
		VDA	52	10	17	277

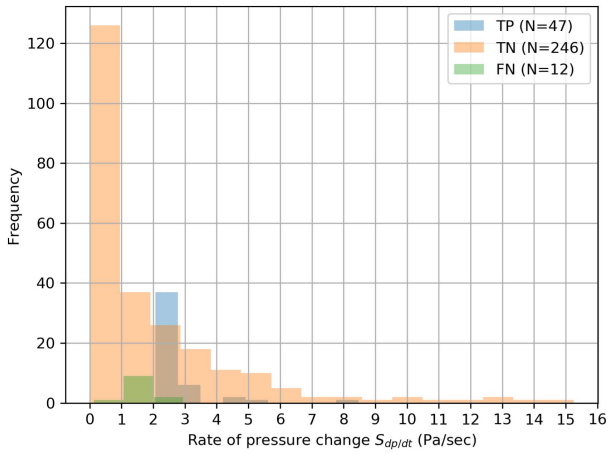

Fig. 4. Distribution of the rate of pressure changes in predicted data in video-annotated data set when using feature set-I.

TABLE IX
CLASSIFICATION RESULTS OF VIDEO-ANNOTATED DATA SET WITH FEATURE SET-I

(a) **Performance metrics**

Class	Precision (%)	Recall (%)	F1-score (%)	Support
HDA	95	100	97	246
VDA	100	80	89	59
weighted average	96	96	96	395

(b) **Confusion matrix**

Class	HDA	VDA	Support
HDA	246	0	246
VDA	12	47	59

in this ablation study. Table X reports the results of the classification performance with features from the following sensor(s): (a) Barometer only, (b) Barometer and tri-axis accelerometer, and (c) Barometer and Wi-Fi scanner (location data). The F_1-score for classifying VDA is 57% (overall accuracy of 89%) with barometer features only. It is significantly improved by adding the tri-axis accelerometer features (overall accuracy of 96% and F_1-score for classifying VDA at 83%). Even

TABLE X
IMPACT OF SENSOR TYPE ON THE CLASSIFIER PERFORMANCE WITH SELECTED FEATURES OF FEATURE SET-I. BARO - BAROMETER, ACC - ACCELEROMETER, AND LOC - LOCATION DATA DERIVED FROM WI-FI SCANNER

Sensor	Overall accuracy (%)	Class	Precision (%)	Recall (%)	F_1-score (%)	Support
Baro.	89	HDA	94	94	94	1899
		VDA	58	56	57	277
Baro + Acc	96	HDA	98	97	98	1899
		VDA	83	84	83	277
Baro + Loc	97	HDA	98	99	99	1899
		VDA	92	88	90	277
Baro + Loc + Acc	98	HDA	99	99	99	1899
		VDA	93	92	93	277

better performance is achieved with the combination of location and barometer features with 97% overall accuracy and 90% F_1-score for classifying VDA. The addition of the accelerometer data to barometer and location data thus only improves the F_1-score by 3%. As noted in Sec. II, previous studies [31], [32] have obtained similar accuracy with accelerometer only or barometer only features. However, their training data was collected in a limited environment (e.g., ambulation only or transportation only activities and short time period). For a data set such as the one considered here, which was collected in a long term free-living environment, it thus seems that barometer only features are not enough to classify VDA with high accuracy; however, adding the data of even one additional sensor data allows excellent performances even in this case.

The XGBoost model (see App. C for a description of the model and its hyperparameters) has an embedded feature ranking method that quantifies the importance of each feature to build the predictive model. The most relevant parameter to quantify relative feature importance is the total gain that measures the improvement in accuracy brought on by the feature for each tree in the model. Based on the total gain, the feature importance of all 95 features is calculated from the tuned model. To understand the impact of using reduced feature sets, we use the top 10 (out of 95) and the top 5 (out of 95) of the important features, denoted as the feature set-II (features 1–10 in Table XI) and feature set-III (features 1–5 in Table XI) respectively. We re-tune the hyperparameters and re-train the classifier model using the same procedure as described in App. D. The reduced feature set size of 10 and 5 are arbitrarily chosen, but it is supported by the fact that the total gain drops drastically after the most important feature ($S_{dp/dt}$) as shown in Table XI.

The classification performance of the XGBoost model with feature sets I, II, and III are shown in Table XII. The overall classification accuracy of the model for all feature sets on the test set stands at 98%, and the F_1-score for classifying VDA is found to be slightly lower at 93% for feature set-I and 92% for feature set-II and III. As the number of features is reduced

TABLE XI
FEATURE IMPORTANCE OBTAINED FROM THE TUNED XGBOOST CLASSIFIER MODEL. TOP 10 RESULTS ARE SHOWN. *S* STANDS FOR SEGMENTED DATA

No	**Feature**	**Total gain**
1	$S_{dp/dt}$	4460
2	$S_{\min(N_{\text{RMS}(\text{std}(M_{acc}))})}$	2614
3	$S_{\min(N_{\text{median}(dx/dt)})}$	988
4	$S_{\min(\widetilde{zcr})}$	421
5	$S_{dx/dt}$	265
6	$S_{\min(N_{\max(M_{acc})})}$	184
7	$S_{\min(N_{\max(dx/dt)})}$	184
8	$S_{\min(N_{\text{avg}(dx/dt)})}$	141
9	$S_{\max(N_{\max(dx/dt)})}$	124
10	$S_{\min(N_{\min(dx/dt)})}$	114

TABLE XII
CLASSIFICATION PERFORMANCE OF THE XGBOOST MODEL

(a) **Performance metrics**

Feature set	Overall accuracy (%)	Class	Precision (%)	Recall (%)	F_1-score (%)	Support
Feature set-I	98	HDA	99	99	99	1899
		VDA	93	92	93	277
Feature set-II	98	HDA	99	99	99	1899
		VDA	93	90	92	277
Feature set-III	98	HDA	98	99	99	1899
		VDA	94	90	92	277

(b) **Confusion matrix**

Feature set	Class	HDA	VDA	Support
Feature set-I	HDA	1870	19	1899
	VDA	22	255	277
Feature set-II	HDA	1870	19	1899
	VDA	27	250	277
Feature set-III	HDA	1874	15	1899
	VDA	29	248	277

from 95 to 10 and ultimately down to 5, there is a slight increase in precision with a complementary decrease in recall. The confusion matrix in Table XIIb shows no significant drop in performance when reducing the feature set size. We use the XGBoost model results with feature set-II in this section's further analysis to balance between performance and the number of features.

D. VDA Classification Performance

Table XIIb shows the confusion matrix—i.e., predicted class distributions and corresponding Type-I (False Positives) and Type-II errors (False Negatives). When closely inspecting the feature space in the test data set, one finds that the Type-II error generally occurs when the rate of pressure changes $S_{dp/dt}$ is small, typically below 1.9 Pa/sec for 65% of the false negatives. This observation may have two possible origins. This is either due to the small magnitude of pressure jumps dp (associated with low recording frequency that splits a single VDA event across multiple time intervals). Alternatively, this could also be due to larger time intervals dt (due to irregular recording frequency of 0.076 $\sim$ 0.016 Hz). The low and irregular sampling rate is the critical limiting factor in both cases. In addition, in some cases, a vertical mobility event follows or precedes a horizontal transportation mode—e.g., above-the-ground or underground train travel—, which may lead to misclassification due to the reliance on Wi-Fi localization to calculate the travel velocity. This is the case, for instance, when the APs are sparse.

E. VDA Recognition Limitations

The magnitude of the altitude change in a given VDA event is derived from the barometric pressure change of the segmented data S_{dp} using Eq (2). The accuracy of this magnitude is limited by the barometric sensor resolution, which is $\pm$12 Pa for our SenSg device (see Table III). Some of the VDA events with lower values of $S_{dp/dt}$ are not appropriately classified, as stated in Sec. V-D. For a typical sampling frequency of 0.062 Hz, this corresponds to an altitude change of 2.5 meters (30 Pa). Hence, it is reasonable to assume that vertical displacements smaller than this value are not properly captured, and thus the vertical moves can only be accurate with a vertical resolution of $\sim$ 2.5 meters.

The classification performance when recognizing VDAs in this study is thus limited by the type of sensor data, sensor resolution, and sampling frequency. For example, location data from GPS with an accuracy of $\pm$10 meters would outperform the often inaccurate Wi-Fi localization, which is only accurate within $\pm$200 meters. Similarly, a higher sampling rate of barometric pressure to the tune of 1 Hz would be ideal compared to the lower sampling frequency of $\sim$ 0.062 Hz in this data set. Moreover, using an accurately annotated data set—e.g., employing video recording—can markedly improve the training performance.

VDA can be further sub-classified into different modes of vertical transportation like elevator, escalator, or stairs. This would, however, require large amounts of video-annotated training data set with high temporal and spatial resolution. This is because the rate of change of vertical displacement—a key metric in distinguishing between these modes [9]—needs to be sampled at a reasonably high resolution, especially to differentiate between stairs climbing and escalator riding. Furthermore, the classification between stairs/escalators and elevators will only be accurate for floor jumps larger than 2 $\sim$ 3 if the sampling frequency is low, such as that found in our data set. For these reasons, we do not consider VDA sub-classification in this study. However, using sensors with a higher sampling rate, such sub-classification of VDA should be attainable, as shown in previous works [26], [31], [32], [75].

F. Prevalence of Vertical Mobility in Singapore's Student Population

We have applied the trained XGBoost model with feature set-II to the curated NSE data described in Table II. The data

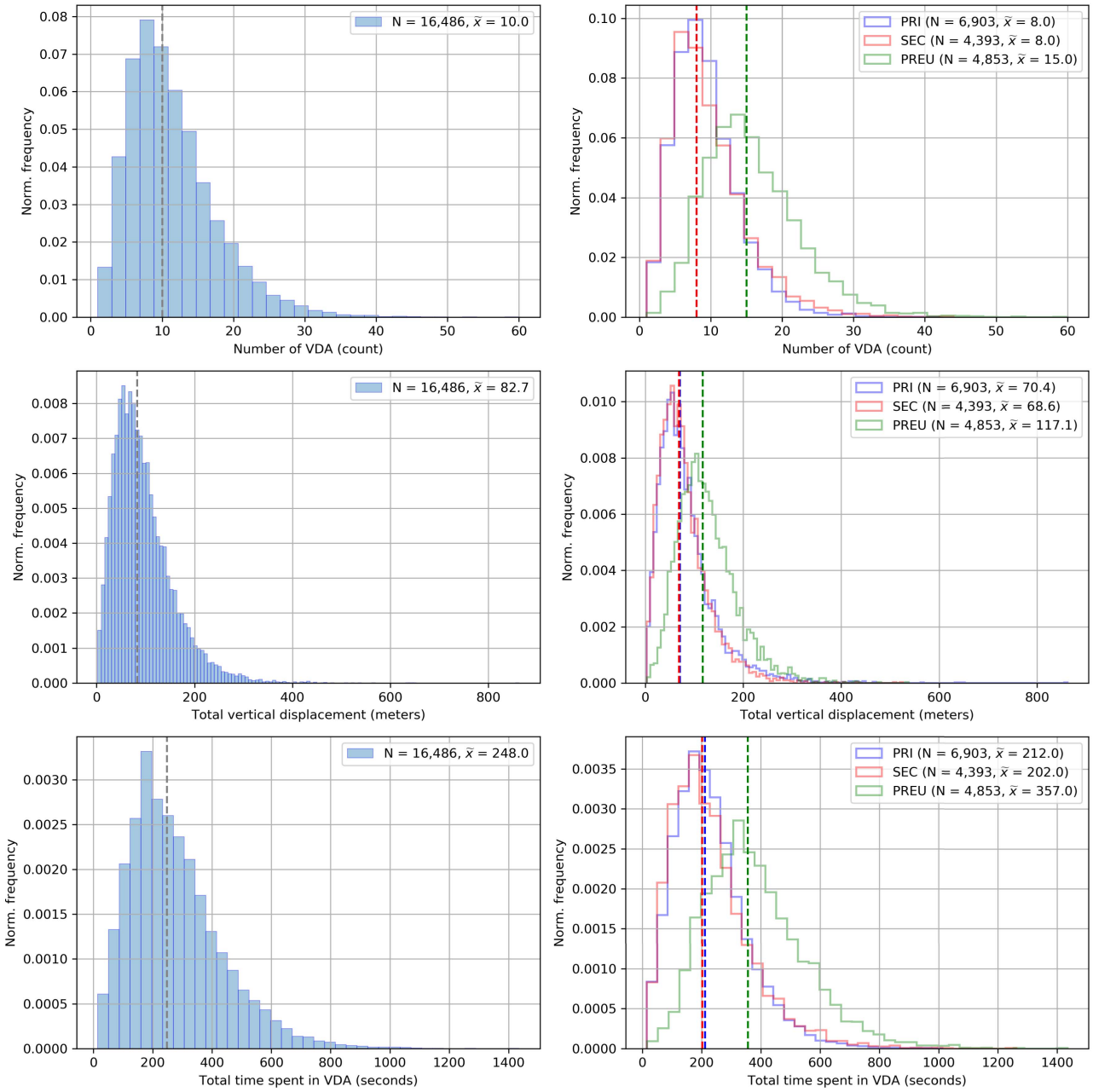

Fig. 5. Aggregated distribution of VDA for a population of $N = 16{,}486$ individuals. The aggregation period is set to 1 day. N is the number of subjects and $\tilde{x}$ denotes the median value (dashed lines). Top row: number of VDA events per subject; Middle row: total cumulated vertical displacement (in meters) per subject; bottom row: total time spent in VDA (in seconds) per subject; left column: total population; right column: subjects grouped by school types.

was collected for $N = 16,486$ students from 89 schools aged 6–19 whose residences and schools were spread throughout the island-state of Singapore. For each subject, the data contains at least 6 hours of coverage during a day. The results presented in this section are aggregated over a single day for each participant—the selected day corresponds to the one with the largest data points collected during their week of carrying the SENSg device as part of the NSE program. In addition, the predicted VDAs are post-processed to remove vertical displacements (less than 9% of total) that are accompanied by significant pressure fluctuations ($dp > 20$ Pa) that may have been caused by sensor errors (see [9]).

The predicted VDAs in the entire data set reaches 182, 841 events after postprocessing. Some statistics of VDA for each subject over a day are calculated and shown in Fig. 5, namely the number of VDAs, the cumulated vertical displacement, and the total time spent in the VDA mode. On a daily average, a subject was found to be engaged in 10 events of vertical mobility, traveled vertically $\sim$ 83 meters, and spent a total of 4 minutes per day in this mode. As an element of comparison, Americans are found to spend on average $\sim$ 65 minutes per day eating [79]. However, the distributions are rather heterogeneous, with individuals who traveled as much as 140 meters vertically in a single VDA event, moved

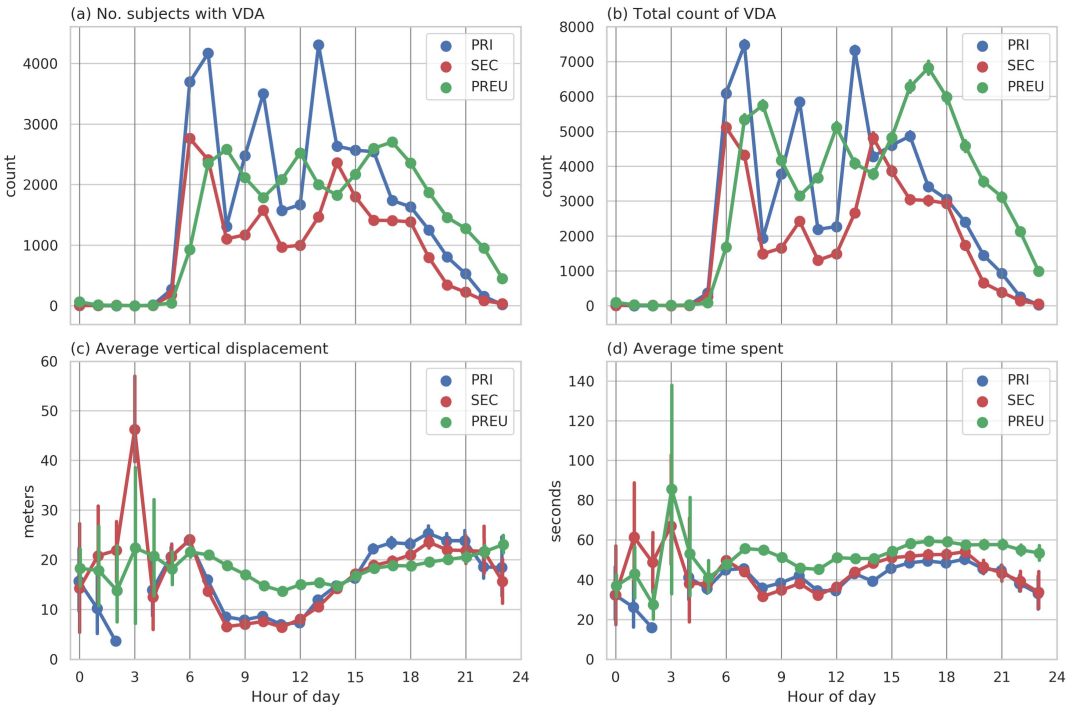

Fig. 6. Temporal statistics of VDA according to group types: (a) number of subjects with VDA (active subjects) by hours, (b) total VDA count by hour, (c) average vertical displacement per active subject by hour, and (d) hourly average time spent in VDA per active subject by hour. The errorbars in (c) and (d) indicate the confidence intervals estimated using a bootstrap approach ($n = 1000$).

up to 60 times in vertical direction and spent up to 24 minutes per day in VDA. The highest vertical displacement in our predicted data (140 meters) is nearly half the size of the highest building in Singapore—the Guoco tower stands at 290 meters.

Fig. 5 also shows the breakdown of the distributions of VDA for primary (PRI), secondary (SEC), and pre-university (PREU) students. Interestingly, the vertical mobility footprint of PREU students is markedly higher than that of PRI or SEC students, even if the descriptive statistics of single VDA events are very similar: the median values are 5.2 m for PRI students, 5.1 m for SEC students, 5.8 m for PREU students; the mean values are respectively 9.3 m (PRI), 8.3 m (SEC), 8.1 m (PREU) and the maximum values are 116 m (PRI), 120 m (SEC), 140 m (PREU). The fact that pre-university students are more active in terms of cumulated VDA can, in particular, be explained by the fact that they are more likely to travel through public transportation like trains that are either above or below the ground road level [80].

The timeline of VDA reveals a rich structure. In highly vertical cities, people experience significant waiting times during their vertical mobility due to shared public transportation such as elevators or slow pedestrian movements in escalators and stairs. In Singapore, these waiting times can be similar in magnitude to the waiting times between trains or buses ($2 \sim 5$ minutes). Businesses operating on appointments only often remind their customers to include the waiting time associated with elevator rides when planning their arrival. While these time scales can still be considered small, the ongoing vertical integration of multi-purpose buildings will underscore the importance of understanding congestion in vertical transportation and mobility. Understanding congestion per land-use type and time is essential to inform better transportation planning, and this point will also apply to vertical transportation.

Fig. 6 shows the hourly statistical distribution of VDA according to the three group types under investigation (PRI, SEC, and PREU). The group-based total number of subjects with VDA (i.e., active subjects, Fig. 6(a)) and total count of VDA (Fig. 6(b)) exhibit similar trends. They indicate that different daily rhythms of individuals occur between the three groups, i.e., the peaks in activity for PRI are at 7 a.m., 10 a.m., 1 p.m., and 4 p.m., SEC at 6 a.m., 10 a.m., 2 p.m., and 6 p.m., and PREU students at 8 a.m., 12 p.m., and 5 p.m. In addition, a large number of activities of PREU students is observed during evening and night times, which can readily be explained by the fact that some schools like the Institute of Technical Education (ITE), operate primarily in the evening and by the active after-school life of the late-teen population.

Due to the low number of active users between 12 a.m. and 5 a.m., the average vertical displacement (Fig. 6(c)) and average time spent in VDA (Fig. 6(d)) show considerable uncertainty within that period and become stable again after 5 a.m. In terms of per-subject average vertical displacement and time spent, the primary and secondary students show similar patterns, while pre-university students yield markedly different patterns. For instance, the primary and secondary students' average vertical displacement is high during the 5 a.m.–6 a.m. time window, drops to 9 meters between

8 a.m.–12 p.m., then peaks up again to $\geq$ 20 meters between 4 p.m.–9 p.m., and decreases after that. On the other hand, the pre-university students' average vertical displacement is about 20 meters between 6 a.m.–7 a.m., and 14 meters around 11 a.m., then slowly increases until 11 p.m. These differences in the morning could be explained by the style of classes between them. Primary and secondary classes are usually fixed, and students do not need to change classes between courses. In contrast, pre-university students will need to move to other classes for different courses.

VI. Conclusion

Over the past two decades, advancements in sensor technology and complexity science have enabled the dissection, with unprecedented accuracy, of the fine details of human mobility in urban areas from large-scale data. Mining these "Big Data" revealed the burstiness and relative predictability of human spatial movements [81], [82], as well as highly dense spatial areas in cities [83]. However, these studies, albeit illuminating, were mainly carried out on large groups of people living and moving about in mostly flat cities and were therefore limited to horizontal movements in two dimensions. The present study explored the application of identifying and monitoring VDA to highlight the prevalence of vertical mobility at city-scale and its potential to add to the understanding of human mobility in general.

This "Big Data" set consisted of 16,581 students between the age of 6 and 19 from 89 schools spread throughout the city-state of Singapore. The relatively long-term tracking (5 days) and high recording frequency (every $\sim$ 16 seconds) have provided high spatiotemporal resolution data sufficient to identify VDA in diverse conditions. The classification performance of the model is similar or closely aligned with the results reported in the literature (Sec. II)—with 98% overall accuracy and 92% F_1-score in classifying VDA—while significantly generalizing its applicability to almost all possible real-world conditions.

The recognition of VDA is instrumental to the effectiveness of a range of critical applications in indoor positioning and navigation [29], [30], [36], [66], estimation of energy expenditure, and health monitoring [16], [39], [47]. The present study markedly expands the scope of applications by rendering possible the performance of large-scale human experiments with the ultimate goal of shedding light on the human mobility patterns in dense urban areas, and their impact on urban planning. Furthermore, the VDA extraction methodology described in this paper can be used to perform urban data analytics. These results may have significant ramifications for the design of dense vertical cities. For instance, using this methodology, one should identify the hidden vertical barriers and possible facilitators to movement in the vertical city. Urban designers and planners would then have quantitative information about the hitherto unknown patterns of vertical human mobility. This new knowledge could prove pivotal to establishing novel design principles that can enhance mobility and, therefore, livability in the vertical urban world.

Our study is ultimately limited by the participants' age group and size, the sensor characteristics (primarily resolution and sampling rate), and the training data collection methods (video annotation versus manual labeling). Future studies can most likely achieve more significant results by improving one or more of these categories to obtain a more accurate and general detection of VDA.

Lastly, aggregated VDA data analysis by population groups/segments has revealed rich details about the anticipated differences in the daily activity profiles between late-teens and younger children. The uncovered patterns of vertical human mobility enabled us to accurately quantify, for the first time, the distance traveled and time spent in vertical transportation in a densely built urban environment. It has also revealed some unique patterns of activity related to vertical transportation that is present in many aspects of our human lives. There is no doubt that a more systematic analysis of the non-aggregated data would provide important new details and unique information about the dynamics of vertical mobility across several dimensions, including gender, age, and socioeconomic status.

Appendix

A. Localization & Interpolation

The location data is obtained using an API from a third-party company called Skyhook based on the available Wi-Fi APs. It requires a minimum number of APs to triangulate a given location. As the density of Wi-Fi APs varies from place to place, accurate localization may not always be achievable with insufficient data. This is especially pronounced in transportation modes—such as underground subway rides, by-pass roads, tunnels, and bridges.—where Wi-Fi APs are sparse or non-existent, even in highly dense cities. In our dataset, a per-person average of 8% data points are missing location information due to failed localization.

An interpolation method is used to predict the missing values to complete the Wi-Fi localization data. As the first step, successfully localized time-series are selected and a fraction of its data is removed randomly. Next, the Root Mean Squared Error (RMSE) value between original and randomly removed data is calculated for three distinct interpolation methods: (1) linear (2) cubic spline, and (3) piece-wise cubic spline to identify the best method. The linear interpolation consistently outperforms other methods under consideration with the lowest RMSE values for a fraction (10 $\sim$ 50%) of the data removed. For example, for fraction$>$ 20% of the data removed, RMSE measured in the degree of latitude/longitude is $\sim$ 0.0001 for linear interpolation while RMSE (degree)$\sim$ 0.005 for other methods.

B. Regression

The Wi-Fi localization data has a low spatial resolution of $\pm$400 meters. The travel velocity estimation based on this data reveals high local errors. A regression model is applied to find the best fit to reduce local fluctuations. To analyze the model performance, RMSE is used to estimate the residuals, and the R-squared value quantifies the proportion of variance explained by the model. The regression model performs poorly when applied to the entire time-series sequence. This is due to the different regions of variability in data. The time series

location data is segmented into a series of local (temporary) variable and global (long-term) variable sequences. The regression model is then applied with different window sizes or knot placements to each of these sequences, a higher number of knots for a global variable sequence and a lower number of knots for a local variable sequence.

A local variable sequence is defined as $S_{i,n} = \{i, i+1, \ldots, n\}$ where the location of index $-\ n$ is at distance $\leq$ distance_cut-off from index $-\ i$. A global variable sequence is created by combining several local variable sequences of length < 10 (~ 2.5 minutes) to reflect long term changes in location.

Two regression models: (1) piece-wise polynomial and (2) natural piece-wise cubic regression spline are considered as well as three smoothing models: (3) Savitzky-Golay smoothing, (4) LOESS model, (5) Exponential smoothing model. These five options are compared against different window sizes or knot placements (local variable $= [5, 15, 30]$, global variable$= [5, 15, 30]$) and distance_cut_off $= [0.1, 0.3, 0.5]$ km). The natural piece-wise Cubic regression spline and Savitzky-Golay show the lowest RMSE and highest R-Squared values for all knot placements/window sizes and distance_cut_off. Either of these methods will suitably reduce the local errors in location data. A low RMSE and high R-squared value can also point to over-fitted data; hence, additional considerations should support model selection. The optimal knot placements should be sparse for local variable data to reduce local fluctuations and denser for global variable data where location varies long-term. Here, Natural Piece-wise cubic regression spline method is selected with knot placements at (local variable, global variable)$= (15, 1)$ of the segmented data using distance_cut_off $= 0.3$ km. Essentially, the knot placements are designed to smooth the local variable data while leaving the global variable sequences intact.

C. Classification Model Parameters

1) XGBoost: Gradient boosting allows an ensemble of weak learners to build models that depend on the gradient descent algorithm to optimize an objective function. The objective function measures the model fitness of the training data and consists of training loss and regularization [84]. Training loss quantifies the model's predictive capability, and the regularization parameters help reduce overfitting by controlling the complexity of the model. The balance between these two terms is commonly known as the bias-variance trade-off [84]. XGBoost classifier model encompasses several parameters that are categorized as general, booster, and learning task parameters [85]. The tree booster parameters allows the specification of learning rate (eta), minimum loss reduction to make a split ($gamma$), maximum depth of a tree (max_depth), minimum sum of weights of all observations in a child (min_child_weight), fraction of observations to be sampled randomly ($subsample$), fraction of columns to be sampled randomly in each tree ($colsample\_bytree$), control of class imbalance ($scale\_pos\_weight$), L2 regularization term on weights (reg_alpha), and L1 regularization term on weights (reg_lambda) [84], [85]. Learning task parameters allows choosing an objective function ($objective$) for optimization against a specified evaluation metric ($eval\_metric$). The number of trees or estimators ($n\_estimators$) required depends on the learning rate eta. Optimizing the tree booster parameters based on the evaluation metric allows the objective function to look for values that avoid over-fitting. Model over-fitting can be further controlled by reducing the learning rate and increasing the number of estimators [85].

2) Random Forest: The Random Forest classifier is an ensemble learning algorithm that tries to create a range of uncorrelated trees by randomly selecting features for each tree and randomly (with replacement) assigning training data to each tree. Both of these properties of Random Forest helps control over-fitting [86], [87]. The parameter $n\_estimators$ gives the number of trees, and the maximum number of features considered for splitting a node is given by $max\_features$. The maximum number of levels in each tree is controlled by the parameter max_depth. The samples given to the tree are controlled by the following parameters: $bootstrap$, min_sample_split, $min\_weight\_fraction\_leaf$, and min_sample_leaf. The parameter $bootstrap$ can be set to $True$ to allow random sampling with replacement. The minimum number of data points assigned to a node before splitting is given by min_sample_split, and the parameter min_sample_leaf is used to control the minimum number of data points allowed in a leaf node. The sample weight can be adjusted using the parameter $min\_weight\_fraction\_leaf$. Finally, the class imbalance in a data set can be controlled by setting the parameter $class\_weight$ to $balanced$.

3) Naive-Bayes: The Naive-Bayes model is a probabilistic learning algorithm based on Bayes' theorem. This study uses the Gaussian Naive-Bayes algorithm that assumes Gaussian distribution for each class [87], [88]. Other Naive-Bayes models such as Multinomial and Bernoulli are defined for discrete data values and hence not suitable for our problem [87]. Gaussian Naive-Bayes model has only two parameters: $var\_smoothing$ and $priors$. The prior probability of the classes can be assigned through $priors$. Since there is no prior probability available for our classes, this parameter is unspecified in this work so that the priors can be learned from the data. The parameter $var\_smoothing$ is used to adjust the weight given to data points far from the mean distribution. This is the only parameter tuned for the Naive-Bayes model here.

4) k-Nearest Neighbors: k-Nearest Neighbors classifier is a class of Nearest Neighbors algorithm that identifies k-nearest training data points based on their similarity [87]. The number of neighbors k is given by the parameter $n\_neighbors$. The neighbors can be weighed uniformly or differently using the parameter $weight$. The distance metric used can be controlled by the parameter p, which denotes the power of the Minkowski distance ($p = 1$ denotes Euclidean and $p = 2$ denotes Manhattan). The speed of finding the nearest neighbors depends on the parameter $algorithm$ that can be set to brute-force or faster methods such as tree-based search algorithms. The tree-based search can be controlled by the parameter $leaf\_size$ that can be adjusted for faster construction and queries.

5) Multilayer Perceptron: The multilayer perceptron is a class of feed-forward artificial neural network models. This supervised learning model uses the backpropagation method that calculates the gradient of a loss function concerning the weights of the network to train the model [89]. It consists of a single input and single output layer and at least one hidden layer. The number of hidden layers and the number of neurons in each hidden layer can be selected using the parameter $hidden\_layer\_sizes$. The neurons can be activated or not using the activation function defined by the parameter $activation$. The weights of the network can be optimized by the solver (e.g., stochastic gradient descent) with the parameter $solver$. Similar to the XGBoost model, the L2 regularization is controlled by $alpha$. Another important parameter for MLP is the $learning\_rate$ that can be a given constant value, scaling value, or an adaptive parameter.

D. Classifier Model Tuning

The four classifier models follow an overall procedural structure for model tuning. The optimal model hyperparameters are selected by grid search and a 5-fold cross-validation using the metric – Area Under the Receiver Operating Characteristic Curve (ROC AUC). The grid search is initialized with hyperparameter values, which are fine tuned until no further change in the results is noticed. The 5-fold cross-validation is used to reduce the bias and efficiently uses the training set to understand the model's predictive power on new data during the tuning procedure. Due to the specific nature of the classifier models, some differences in the procedure exist. For example, all the hyperparameters for the Random Forest, Naive-Bayes, and k-Nearest Neighbors are tuned using a single grid search. In contrast, the hyperparameters for XGBoost are tuned in a series of grid searches. The following steps thus tune the XGBoost model:

XGBoost Model Tuning Steps: The optimal parameter values are calculated in a series of steps, where each step progresses by estimating the parameter under consideration based on the parameters calculated from the preceding step. The steps taken to tune the model are as follows: (1) Set a high learning rate and find the optimal number of estimators, (2) For the given learning rate and the number of estimators, find optimal max_depth and min_child_weight, (3) Find the optimal value of $gamma$ (4) Re-calibrate the optimal number of estimators, (5) find optimal values for the parameters $subsample$ and $colsample\_bytree$, (6) find the optimal values for the regularization parameters reg_alpha and reg_lambda, (7) Re-calibrate the optimal number of estimators, (8) Reduce the learning rate and find the optimal number of estimators [85].

The cross-entropy loss for binary classification is set as the objective function. The above steps are followed for an initial learning rate of 0.3 from (1) to (7). As the final step (8), the learning rate is reduced considerably (from 0.3 to 0.2 for feature set-I, to 0.1 for both feature set-II and feature set-III) to control over-fitting while keeping the F_1 score of VDA classification higher. The optimal number of estimators is then found to be 43, 125, and 72 for feature set-I, II, and III, respectively, from 5-fold cross-validation for the given learning rate. The class imbalance is acknowledged by setting the parameter $scale\_pos\_weight$ to 1 for faster convergence.

E. Pressure-Altitude Relation

The fundamental equation for fluids at rest dictates the relationship between atmospheric pressure and altitude [90]. The change in altitude is indeed given by

$$z_2 - z_1 = -\frac{p_2 - p_1}{\gamma}, \tag{2}$$

where $\gamma = \rho g$ is the specific weight of air with density $\rho = 1.225$ kg/m^3 and g is the acceleration due to gravity $g = 9.81$ m/s^2 at standard sea-level conditions. The fluid is assumed to be incompressible and in isothermal conditions. This pressure-altitude equation is valid for data collected for elevation less than 10 km from sea level [90], which is always the case in our study.

Acknowledgment

On-time production of the sensors was only possible due to strong support from Delta Electronics DRC, IABG, and Taoyuan Factory. Logistics for the distribution of thousands of sensors was facilitated by the Singapore Science Center, and the infrastructure to securely store the data was built and maintained by the A*STAR Institute for High Performance Computing.

The authors would like to thank Francisco Benita, Francesco Scandola, and Garvit Bansal for their assistance with SENSg devices and guidance on data collection. They would also like to thank the National Research Foundation (NRF) of Singapore for providing access to the National Science Experiment data.

References

[1] Y. Zhou, *et al.*, "Understanding urban human mobility through crowdsensed data," *IEEE Commun. Mag.*, vol. 56, no. 11, pp. 52–59, Nov. 2018.

[2] E. Wilhelm, *et al.*, "Wearable environmental sensors and infrastructure for mobile large-scale urban deployment," *IEEE Sensors J.*, vol. 16, no. 22, pp. 8111–8123, Nov. 2016.

[3] Y. Zhou, B. P. L. Lau, C. Yuen, B. Tuncer, and E. Wilhelm, "Understanding urban human mobility through crowdsensed data," *IEEE Commun. Mag.*, vol. 56, no. 11, pp. 52–59, Nov. 2018.

[4] A. G. Yeh and B. Yuen, *Introduction: High-Rise Living in Asian Cities*. Dordrecht, The Netherlands: Springer, 2011, pp. 1–8.

[5] S. Gopalakrishnan, D. Wong, A. Manivannan, R. Bouffanais, and T. Schroepfer, "User-driven emergent patterns of space use in vertically integrated urban environments," in *Proc. 21st Int. Conf. Architectural Res. Centers Consortium (ARCC)*, Phoenix, AZ, USA, 2021, pp. 215–222. [Online]. Available: http://www.arcc-arch.org/wp-content/uploads/2021/08/ARCC-2021-Proceedings_Digital-Version_Web_PP.pdf

[6] R. Bouffanais and L. Sun Sun. (2019). *The Rise of Homo Verticalis*. Accessed: Feb. 22, 2022. [Online]. Available: https://blogs.scientificamerican.com/observations/the-rise-of-homo-verticalis/

[7] H. Barbosa *et al.*, "Human mobility: Models and applications," *Phys. Rep.*, vol. 734, pp. 1–74, Mar. 2018.

[8] S. Hasan, C. Schneider, S. V. Ukkusuri, and M. C. González, "Spatiotemporal patterns of urban human mobility," *J. Statist. Phys.*, vol. 151, nos. 1–2, pp. 304–318, Apr. 2013.

[9] A. Manivannan, W. C. B. Chin, A. Barrat, and R. Bouffanais, "On the challenges and potential of using barometric sensors to track human activity," *Sensors*, vol. 20, no. 23, p. 6786, Nov. 2020.

[10] M. Straczkiewicz, P. James, and J.-P. Onnela, "A systematic review of smartphone-based human activity recognition for health research," 2019, *arXiv:1910.03970*.

[11] O. D. Lara and M. A. Labrador, "A survey on human activity recognition using wearable sensors," *IEEE Commun. Surveys Tuts.*, vol. 15, no. 3, pp. 1192–1209, 3rd Quart., 2013.

[12] A. Bulling, U. Blanke, and B. Schiele, "A tutorial on human activity recognition using body-worn inertial sensors," *ACM Comput. Surv.*, vol. 46, no. 3, p. 33, 2014.

[13] K. Sagawa, T. Ishihara, A. Ina, and H. Inooka, "Classification of human moving patterns using air pressure and acceleration," in *Proc. 24th Annu. Conf. IEEE Ind. Electron. Soc.*, vol. 2, Aug./Sep. 1998, pp. 1214–1219.

[14] M. Janidarmian, A. Roshan Fekr, K. Radecka, and Z. Zilic, "A comprehensive analysis on wearable acceleration sensors in human activity recognition," *Sensors*, vol. 17, no. 3, p. 529, Mar. 2017.

[15] N. Twomey *et al.*, "A comprehensive study of activity recognition using accelerometers," *Informatics*, vol. 5, no. 2, p. 27, 2018.

[16] M. Saleh, M. Abbas, and R. B. Le Jeannes, "FallAllD: An open dataset of human falls and activities of daily living for classical and deep learning applications," *IEEE Sensors J.*, vol. 21, no. 2, pp. 1849–1858, Jan. 2021.

[17] Y. Chen and C. Shen, "Performance analysis of smartphone-sensor behavior for human activity recognition," *IEEE Access*, vol. 5, pp. 3095–3110, 2017.

[18] J. Mäntyjärvi, J. Himberg, and T. Seppänen, "Recognizing human motion with multiple acceleration sensors," in *Proc. IEEE Int. Conf. Syst., Man Cybern. e-Syst. e-Man Cybern. Cyberspace*, vol. 2, Oct. 2001, pp. 747–752.

[19] S. Chung, J. Lim, K. J. Noh, G. Kim, and H. Jeong, "Sensor data acquisition and multimodal sensor fusion for human activity recognition using deep learning," *Sensors*, vol. 19, no. 7, p. 1716, Apr. 2019.

[20] K. Kunze and P. Lukowicz, "Sensor placement variations in wearable activity recognition," *IEEE Pervasive Comput.*, vol. 13, no. 4, pp. 32–41, Oct. 2014.

[21] M. Cornacchia, K. Ozcan, Y. Zheng, and S. Velipasalar, "A survey on activity detection and classification using wearable sensors," *IEEE Sensors J.*, vol. 17, no. 2, pp. 386–403, Jan. 2017.

[22] L. Cong, J. Tian, and H. Qin, "A practical floor localization algorithm based on multifeature motion mode recognition utilizing FM radio signals and inertial sensors," *IEEE Sensors J.*, vol. 20, no. 15, pp. 8806–8819, Aug. 2020.

[23] S. Boim, G. Even-Tzur, and I. Klein, "Height difference determination using smartphones based accelerometers," *IEEE Sensors J.*, early access, Mar. 2, 2021, doi: 10.1109/JSEN.2021.3062346.

[24] Z. Yan, V. Subbaraju, D. Chakraborty, A. Misra, and K. Aberer, "Energy-efficient continuous activity recognition on mobile phones: An activity-adaptive approach," in *Proc. 16th Int. Symp. Wearable Comput.*, Jun. 2012, pp. 17–24.

[25] L. Bao and S. S. Intille, "Activity recognition from user-annotated acceleration data," in *Pervasive Computing*, vol. 3001. Berlin, Germany: Springer, 2004, ch. 1, pp. 1–17.

[26] M. Liu, H. Li, Y. Wang, F. Li, and X. Chen, "Double-windows-based motion recognition in multi-floor buildings assisted by a built-in barometer," *Sensors*, vol. 18, no. 4, p. 1061, Apr. 2018.

[27] A. Moncada-Torres, K. Leuenberger, R. Gonzenbach, A. Luft, and R. Gassert, "Activity classification based on inertial and barometric pressure sensors at different anatomical locations," *Physiol. Meas.*, vol. 35, no. 7, p. 1245, 2014.

[28] A. El Halabi and H. Artail, "Integrating pressure and accelerometer sensing for improved activity recognition on smartphones," in *Proc. 3rd Int. Conf. Commun. Inf. Technol. (ICCIT)*, Jun. 2013, pp. 121–125.

[29] M. Ji, J. Liu, X. Xu, and Z. Lu, "The improved 3D pedestrian positioning system based on foot-mounted inertial sensor," *IEEE Sensors J.*, vol. 21, no. 22, pp. 25051–25060, Nov. 2021.

[30] Y. Zhao, J. Liang, Y. Cui, X. Sha, and W. J. Li, "Adaptive 3D position estimation of pedestrians by wearing one ankle sensor," *IEEE Sensors J.*, vol. 20, no. 19, pp. 11642–11651, Oct. 2020.

[31] K. Muralidharan, A. J. Khan, A. Misra, R. K. Balan, and S. Agarwal, "Barometric phone sensors: More hype than hope!" in *Proc. 15th Workshop Mobile Comput. Syst. Appl.*, 2014, p. 12.

[32] S. Vanini, F. Faraci, A. Ferrari, and S. Giordano, "Using barometric pressure data to recognize vertical displacement activities on smartphones," *Comput. Commun.*, vol. 87, pp. 37–48, Aug. 2016.

[33] S.-M. Lee, S. Min Yoon, and H. Cho, "Human activity recognition from accelerometer data using convolutional neural network," in *Proc. IEEE Int. Conf. Big Data Smart Comput. (BigComp)*, Feb. 2017, pp. 131–134.

[34] I. Cleland, M. P. Donnelly, C. D. Nugent, J. Hallberg, M. Espinilla, and M. Garcia-Constantino, "Collection of a diverse, realistic and annotated dataset for wearable activity recognition," in *Proc. IEEE Int. Conf. Pervasive Comput. Commun. Workshops (PerCom Workshops)*, Mar. 2018, pp. 555–560.

[35] C. Bollmeyer, T. Esemann, H. Gehring, and H. Hellbruck, "Precise indoor altitude estimation based on differential barometric sensing for wireless medical applications," in *Proc. IEEE Int. Conf. Body Sensor Netw.*, May 2013, pp. 1–6.

[36] G. Pipelidis, O. R. M. Rad, D. Iwaszczuk, C. Prehofer, and U. Hugentobler, "A novel approach for dynamic vertical indoor mapping through crowd-sourced smartphone sensor data," in *Proc. Int. Conf. Indoor Positioning Indoor Navigat. (IPIN)*, Sep. 2017, pp. 1–8.

[37] A. M. Sabatini and V. Genovese, "A sensor fusion method for tracking vertical velocity and height based on inertial and barometric altimeter measurements," *Sensors*, vol. 14, no. 8, pp. 13324–13347, Aug. 2014.

[38] B. Ghimire, C. Nickel, and J. Seitz, "Pedestrian motion state classification using pressure sensors," in *Proc. Int. Conf. Indoor Positioning Indoor Navigat. (IPIN)*, Oct. 2016, pp. 1–6.

[39] F. Bianchi, S. J. Redmond, M. R. Narayanan, S. Cerutti, and N. H. Lovell, "Barometric pressure and triaxial accelerometry-based falls event detection," *IEEE Trans. Neural Syst. Rehabil. Eng.*, vol. 18, no. 6, pp. 619–627, Dec. 2010.

[40] M. Voleno, S. J. Redmond, S. Cerutti, and N. H. Lovell, "Energy expenditure estimation using triaxial accelerometry and barometric pressure measurement," in *Proc. Annu. Int. Conf. IEEE Eng. Med. Biol.*, Aug. 2010, pp. 5185–5188.

[41] F. Massé, R. R. Gonzenbach, A. Arami, A. Paraschiv-Ionescu, A. R. Luft, and K. Aminian, "Improving activity recognition using a wearable barometric pressure sensor in mobility-impaired stroke patients," *J. Neuroeng. Rehabil.*, vol. 12, no. 1, p. 72, Dec. 2015.

[42] C. Moufawad el Achkar, C. Lenoble-Hoskovec, A. Paraschiv-Ionescu, K. Major, C. Büla, and K. Aminian, "Instrumented shoes for activity classification in the elderly," *Gait Posture*, vol. 44, pp. 12–17, Feb. 2016.

[43] M. Elhoushi, J. Georgy, A. Wahdan, M. Korenberg, and A. Noureldin, "Using portable device sensors to recognize height changing modes of motion," in *Proc. IEEE Int. Instrum. Meas. Technol. Conf. (I2MTC)*, May 2014, pp. 477–481.

[44] C. Figueira, R. Matias, and H. Gamboa, "Body location independent activity monitoring," in *Proc. 9th Int. Joint Conf. Biomed. Eng. Syst. Technol.*, 2016, pp. 190–197.

[45] F. Taia Alaoui, H. Fourati, A. Kibangou, B. Robu, and N. Vuillerme, "Urban transportation mode detection from inertial and barometric data in pedestrian mobility," *IEEE Sensors J.*, early access, Mar. 12, 2021, doi: 10.1109/JSEN.2021.3065848.

[46] A. Ejupi, C. Galang, O. Aziz, E. J. Park, and S. Robinovitch, "Accuracy of a wavelet-based fall detection approach using an accelerometer and a barometric pressure sensor," in *Proc. 39th Annu. Int. Conf. IEEE Eng. Med. Biol. Soc. (EMBC)*, Jul. 2017, pp. 2150–2153.

[47] K. Leuenberger, R. Gonzenbach, E. Wiedmer, A. Luft, and R. Gassert, "Classification of stair ascent and descent in stroke patients," in *Proc. 11th Int. Conf. Wearable Implant. Body Sensor Netw. Workshops*, Jun. 2014, pp. 11–16.

[48] K. Sankaran, M. Zhu, X. F. Guo, A. L. Ananda, M. C. Chan, and L.-S. Peh, "Using mobile phone barometer for low-power transportation context detection," in *Proc. 12th ACM Conf. Embedded Netw. Sensor Syst.*, Nov. 2014, pp. 191–205.

[49] M. Monteiro and A. C. Marti, "Using smartphone pressure sensors to measure vertical velocities of elevators, stairways, and drones," 2016, *arXiv:1607.00363*.

[50] M. Wu, P. H. Pathak, and P. Mohapatra, "Monitoring building door events using barometer sensor in smartphones," in *Proc. ACM Int. Joint Conf. Pervasive Ubiquitous Comput. (UbiComp)*, 2015, pp. 319–323.

[51] J. Wang, Y. Chen, S. Hao, X. Peng, and L. Hu, "Deep learning for sensor-based activity recognition: A survey," *Pattern Recognit. Lett.*, vol. 119, pp. 3–11, Mar. 2019. [Online]. Available: http://www.sciencedirect.com/science/article/pii/S016786551830045X

[52] H. F. Nweke, Y. W. Teh, M. A. Al-Garadi, and U. R. Alo, "Deep learning algorithms for human activity recognition using mobile and wearable sensor networks: State of the art and research challenges," *Expert Syst. Appl.*, vol. 105, pp. 233–261, Sep. 2018.

[53] F. Attal *et al.*, "Physical human activity recognition using wearable sensors," *Sensors*, vol. 15, no. 12, pp. 31314–31338, 2015.

[54] E. Ramanujam, T. Perumal, and S. Padmavathi, "Human activity recognition with smartphone and wearable sensors using deep learning techniques: A review," *IEEE Sensors J.*, vol. 21, no. 12, pp. 13029–13040, Jun. 2021.

[55] SUTD. (2016). *National Science Experiment*. Singapore. Accessed: Feb. 22, 2022. [Online]. Available: https://www.family.sg/singapore-national-science-experiment.html
[56] E. Wilhelm *et al.*, "Wearable environmental sensors and infrastructure for mobile large-scale urban deployment," *IEEE Sensors J.*, vol. 16, no. 22, pp. 8111–8123, Nov. 2016.
[57] Y. Zhou, J. Wang, P. Shi, D. Dahlmeier, N. Tippenhauer, and E. Wilhelm, "Power-saving transportation mode identification for large-scale applications," 2017, *arXiv:1701.05768*.
[58] Skyhook. (2021). *Skyhook Location Services*. Accessed: Feb. 22, 2022. [Online]. Available: https://www.skyhook.com/
[59] J. He, Q. Zhang, L. Wang, and L. Pei, "Weakly supervised human activity recognition from wearable sensors by recurrent attention learning," *IEEE Sensors J.*, vol. 19, no. 6, pp. 2287–2297, Mar. 2019.
[60] S. Hyuga, M. Ito, M. Iwai, and K. Sezaki, "Estimate a user's location using smartphone's barometer on a subway," in *Proc. 5th Int. Workshop Mobile Entity Localization Tracking GPS-Less Environments*, Nov. 2015, p. 2.
[61] H. Xia, X. Wang, Y. Qiao, J. Jian, and Y. Chang, "Using multiple barometers to detect the floor location of smart phones with built-in barometric sensors for indoor positioning," *Sensors*, vol. 15, no. 4, pp. 7857–7877, 2015.
[62] H. Ye, T. Gu, X. Tao, and J. Lu, "Scalable floor localization using barometer on smartphone," *Wireless Commun. Mobile Comput.*, vol. 16, no. 16, pp. 2557–2571, Nov. 2016.
[63] B.-J. Ho, P. Martin, P. Swaminathan, and M. Srivastava, "From pressure to path: Barometer-based vehicle tracking," in *Proc. 2nd ACM Int. Conf. Embedded Syst. Energy-Efficient Built Environments*, 2015, pp. 65–74.
[64] M. B. Del Rosario *et al.*, "A comparison of activity classification in younger and older cohorts using a smartphone," *Physiol. Meas.*, vol. 35, no. 11, p. 2269, 2014.
[65] M. Tachikawa, T. Maekawa, and Y. Matsushita, "Predicting location semantics combining active and passive sensing with environment-independent classifier," in *Proc. ACM Int. Joint Conf. Pervasive Ubiquitous Comput.*, Sep. 2016, pp. 220–231.
[66] F. Haque, V. Dehghanian, A. O. Fapojuwo, and J. Nielsen, "A sensor fusion-based framework for floor localization," *IEEE Sensors J.*, vol. 19, no. 2, pp. 623–631, Jan. 2019.
[67] F. Zhao, H. Luo, X. Zhao, Z. Pang, and H. Park, "HYFI: Hybrid floor identification based on wireless fingerprinting and barometric pressure," *IEEE Trans. Ind. Informat.*, vol. 13, no. 1, pp. 330–341, Feb. 2017.
[68] Z. Wang, M. Jiang, Y. Hu, and H. Li, "An incremental learning method based on probabilistic neural networks and adjustable fuzzy clustering for human activity recognition by using wearable sensors," *IEEE Trans. Inf. Technol. Biomed.*, vol. 16, no. 4, pp. 691–699, Jul. 2012.
[69] Y. Nam and J. W. Park, "Child activity recognition based on cooperative fusion model of a triaxial accelerometer and a barometric pressure sensor," *IEEE J. Biomed. Health Informat.*, vol. 17, no. 2, pp. 420–426, Mar. 2013.
[70] C. Wang *et al.*, "Low-power fall detector using triaxial accelerometry and barometric pressure sensing," *IEEE Trans. Ind. Informat.*, vol. 12, no. 6, pp. 2302–2311, Dec. 2016.
[71] P. Anastasopoulou, M. Tansella, J. Stumpp, L. Shammas, and S. Hey, "Classification of human physical activity and energy expenditure estimation by accelerometry and barometry," in *Proc. Annu. Int. Conf. IEEE Eng. Med. Biol. Soc.*, Aug. 2012, pp. 6451–6454.
[72] Z. Xu, J. Wei, J. Zhu, and W. Yang, "A robust floor localization method using inertial and barometer measurements," in *Proc. Int. Conf. Indoor Positioning Indoor Navigat. (IPIN)*, Sep. 2017, pp. 1–8.
[73] N. Kronenwett, S. Qian, K. Mueller, and G. F. Trommer, "Elevator and escalator classification for precise indoor localization," in *Proc. Int. Conf. Indoor Positioning Indoor Navigat. (IPIN)*, Sep. 2018, pp. 1–8.
[74] A. Dimri, H. Singh, N. Aggarwal, B. Raman, D. Bansal, and K. K. Ramakrishnan, "RoadSphygmo: Using barometer for traffic congestion detection," in *Proc. 8th Int. Conf. Commun. Syst. Netw. (COMSNETS)*, Jan. 2016, pp. 1–8.
[75] C. Lang and S. Kaiser, "Classifying elevators and escalators in 3D pedestrian indoor navigation using foot-mounted sensors," in *Proc. Int. Conf. Indoor Positioning Indoor Navigat. (IPIN)*, Sep. 2018, pp. 1–7.
[76] R. Ichikari, L. C. M. Ruiz, M. Kourogi, T. Kurata, T. Kitagawa, and S. Yoshii, "Indoor floor-level detection by collectively decomposing factors of atmospheric pressure," in *Proc. Int. Conf. Indoor Positioning Indoor Navigat. (IPIN)*, Oct. 2015, pp. 1–11.
[77] Y. Li, Z. Gao, Z. He, P. Zhang, R. Chen, and N. El-Sheimy, "Multi-sensor multi-floor 3D localization with robust floor detection," *IEEE Access*, vol. 6, pp. 76689–76699, 2018.
[78] G. Zheng, "A novel attention-based convolution neural network for human activity recognition," *IEEE Sensors J.*, vol. 21, no. 23, pp. 27015–27025, Dec. 2021.
[79] K. Hamrick and K. J. Shelley, "How much time do Americans spend preparing and eating food?" in *Amber Waves:The Economics of Food, Farming, Natural Resources, and Rural America*. Washington, DC, USA: US Department of Agriculture (USDA), Economic Research Service, 2005. [Online]. Available: https://EconPapers.repec.org/RePEc:ags:uersaw:127415
[80] B. Monnot, F. Benita, and G. Piliouras, "How bad is selfish routing in practice?" 2017, *arXiv:1703.01599*.
[81] A.-L. Barabási, *Bursts: Hidden Patterns Behind Everything We Do, From Your e-Mail to Bloody Crusades*. Baltimore, MD, USA: Penguin, 2010.
[82] M. C. González, C. A. Hidalgo, and A.-L. Barabási, "Understanding individual human mobility patterns," *Nature*, vol. 453, no. 7196, pp. 779–782, 2008.
[83] E. J. Willemse, B. Tunçer, and R. Bouffanais, "Identifying highly dense areas from raw location data," in *Proc. 24th Int. Conf. Assoc. Comput.-Aided Architectural Design Res. Asia*, vol. 2, 2019, pp. 805–814.
[84] XGBoost. (2020). *XGBoost Documentation*. Accessed: Feb. 22, 2022. [Online]. Available: https://xgboost.readthedocs.io/
[85] A. Jain. (2020). *XGBoost Parameter Tuning Guide to Parameter Tuning in XGBoost*. Accessed: Feb. 22, 2022. [Online]. Available: https://www.analyticsvidhya.com/blog/2016/03/complete-guide-parameter-tuning-xgboost-with-codes-python/
[86] T. Yiu. (2019). *Understanding Random Forest*. Accessed: Feb. 22, 2022. [Online]. Available: https://towardsdatascience.com/understanding-random-forest-58381e0602d2
[87] F. Pedregosa *et al.*, "Scikit-learn: Machine learning in Python," *J. Mach. Learn. Res.*, vol. 12, pp. 2825–2830, Jan. 2011.
[88] A. Sharma. (2021). *Gaussian Naive Bayes With Hyperparameter Tuning*. Accessed: Feb. 22, 2022. [Online]. Available: https://www.analyticsvidhya.com/blog/2021/01/gaussian-naive-bayes-with-hyperpameter-tuning/
[89] J. Friedman *et al.*, *The Elements of Statistical Learning* (Springer Series in Statistics) vol. 1, no. 10. New York, NY, USA: Springer, 2001.
[90] D. F. Young, B. R. Munson, T. H. Okiishi, and W. W. Huebsch, *A Brief Introduction to Fluid Mechanics*. Hoboken, NJ, USA: Wiley, 2010.

Ajaykumar Manivannan received the B.Eng. degree in aerospace engineering from Hindustan University, India, in 2013, and the M.Sc. degree in aerospace engineering from Technische Universität München (TUM), Germany, and Nanyang Technological University (NTU), Singapore, in 2016. He is currently pursuing the Ph.D. degree with the Department of Mechanical Engineering, University of Ottawa, Ottawa, ON, Canada. His research interests include computational social science, human mobility, network science, and fluid mechanics.

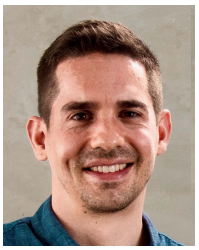

Elias J. Willemse received the B.Eng. and Ph.D. degrees in industrial engineering from the University of Pretoria, Pretoria, South Africa, in 2007 and 2016, respectively. He was a Senior Lecturer at the University of Pretoria, Pretoria, from 2016 to 2019. He was a Postdoctoral Researcher with the Singapore University of Technology and Design, Singapore, from 2018 to 2020. He is currently the CTO of Waste Labs. His research interests include optimization modeling, and their application to transportation and waste collection systems.

Balamurali B. T. received the Ph.D. degree in electrical and computer engineering from the University of Auckland, New Zealand, in 2015. After his Ph.D. degree, he worked as a Researcher at the Gastro Intestinal Group, Auckland Bioengineering Institute. He was also a Lecturer at the Auckland University of Technology. Prior to his Ph.D. endeavor, he was a Senior Design and a Development Engineer at Tata Elxsi, India. He is currently a Postdoctoral Research Fellow working at the Singapore University of Technology and Design. He is passionate about artificial intelligence and trying to solve a variety of problems related to bio-acoustics processing, detection and classification of bio-signals, automatic speech/speaker recognition, spoofed-speech detection, blacklisted speaker identification, blind source separation, music classification, fluid flow classification, and early-dementia prediction.

Wei Chien Benny Chin received the B.Sc., M.Sc., and Ph.D. degrees in geography from the National Taiwan University, Taiwan, in 2011, 2014, and 2018, respectively. He is currently a Postdoctoral Researcher with the Singapore University of Technology and Design. He is also participating in projects associated with complex human movement and the horizontal and vertical dimensions of spatial structures. His research interests include space-time analysis and complex network analysis.

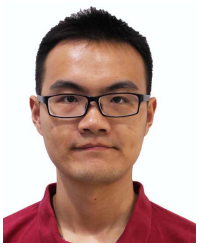

Yuren Zhou received the B.Eng. degree in electrical engineering from the Harbin Institute of Technology, Harbin, China, in 2014, and the Ph.D. degree in engineering from the Singapore University of Technology and Design, Singapore, in 2019. His research interests include data mining, machine learning, and their applications in human mobility, building energy management, and the Internet of Things.

Bige Tunçer received the B.Arch. degree from Middle East Technical University in 1993, the M.Sc. degree from Carnegie Mellon University in 1996, and the Ph.D. degree from the Delft University of Technology in 2009. She is now an Associate Professor at the Singapore University of Technology and Design, where she leads the Informed Design Laboratory. The lab's research focuses on data driven architectural and urban design. She leads and participates in large multi-disciplinary research projects in evidence informed design, the IoT, and big data.

Alain Barrat received the B.Sc. and M.Sc. degrees in physics from École Normale Supérieure, Paris, France, in 1992 and 1994, respectively, and the Ph.D. degree in theoretical physics from UPMC University, Paris, in 1996. He was a Postdoctoral Fellow at the Abdus Salam ICTP, Trieste, Italy, and entered the French National Council for Scientific Research (CNRS) as a Junior Researcher in 1998. He is currently a CNRS Senior Researcher at the Centre de Physique Théorique, Marseille, France. Since April 2019, he has been a Specially Appointed Professor at the Tokyo Tech World Research Hub Initiative, Tokyo, Japan. His research interests include statistical physics and its interdisciplinary applications. He is an expert in the field of complex networks, from fundamental aspects to applications ranging from computational social science to epidemiology.

Roland Bouffanais (Member, IEEE) received the B.Sc. and M.Sc. degrees in physics from École Normale Supérieure (ENS Lyon), Lyon, France, in 1997 and 1999, respectively, the M.Sc. degree in physics from UPMC Paris Sorbonne University, Paris, France, in 1999, and the Ph.D. degree in engineering from the École Polytechnique Fédérale de Lausanne (EPFL), Lausanne, Switzerland, in 2007. He was a Postdoctoral Fellow and an Associate with the Department of Mechanical Engineering, Massachusetts Institute of Technology (MIT), Cambridge, MA, USA. He is now an Associate Professor with the Department of Mechanical Engineering, University of Ottawa, Ottawa, ON, Canada. His interdisciplinary research spans a vast breadth of areas and focused on the design and control of decentralized complex systems, multi-agent systems, leader–follower consensus dynamics, and non-linear dynamical systems.